Morphometric changes with age in human trabecular bone structural units (BSU) of the lumbar spine

by

Britney A. Lamarche

A thesis submitted in partial fulfillment
of the requirements for the degree of
Master of Applied Science (MASc) in Engineering Science

The Faculty of Graduate Studies
Laurentian University
Sudbury, Ontario, Canada

THESIS DEFENCE COMMITTEE/COMITÉ DE SOUTENANCE DE THÈSE
Laurentian Université/Université Laurentienne
Faculty of Graduate Studies/Faculté des études supérieures

Title of Thesis Titre de la thèse	Morphometric changes with age in human trabecular bone structural units (BSU) of the lumbar spine
Name of Candidate Nom du candidat	Lamarche, Britney
Degree Diplôme	Master of Science
Department/Program Département/Programme	Engineering Science
Date of Defence Date de la soutenance	November 20, 2020

APPROVED/APPROUVÉ

Thesis Examiners/Examinateurs de thèse:

Dr. Brent Lievers
(Supervisor/Directeur de thèse)

Dr. Brahim Chebbi
(Committee member/Membre du comité)

Dr. Krishna Challagulla
(Committee member/Membre du comité)

Dr. Kathryn Grandfield
(External Examiner/Examinateur externe)

Approved for the Faculty of Graduate Studies
Approuvé pour la Faculté des études supérieures
Dr. Lace Marie Brogden
Madame Lace Marie Brogden
Acting Dean, Faculty of Graduate Studies
Doyen intérimaire, Faculté des études supérieures

ACCESSIBILITY CLAUSE AND PERMISSION TO USE

Abstract

Age-related fractures are common at skeletal sites with high proportions of cancellous bone such as the hip and spine. Research has shown that measures of bone quantity alone are imperfect predictors of fracture risk, so recent efforts have focused on combining them with measures of bone quality. One aspect of quality that has received little attention is the microstructure of the trabeculae themselves, which are composed of a patchwork of bone structural units (BSU), also known as hemiosteons or trabecular packets, bonded together by cement lines. Any changes in the size of the BSU can be expected to affect the mechanical and failure behavior of cancellous bone. The present work quantified morphometric changes in BSU from the vertebra of 8 young and 8 old individuals as a function of age and 3-D architectural parameters. Reductions in the size of BSU and increases in the proportion of cement line were found to occur with ageing, but these changes were more highly correlated to deteriorating cancellous architecture. These relationships, and the mechanical implications of smaller BSU and increased amounts of brittle cement line, require further investigation.

Keywords: Bone structural units (BSU); cancellous bone; trabecular packets, trabecular architecture; histomorphometry

Acknowledgements

First, I would like to thank my supervisor Dr. Brent Lievers. Since approaching me with this project, you've always offered guidance and support, while allowing me to work through problems and improve my critical thinking skills. I truly appreciate your patience and all the work you put into helping me succeed, both academically, and professionally. Having you as a mentor has without a doubt helped me grow as a researcher and engineer, and I attribute any of my future successes in part to you.

To Thomas, Christina, and the other researchers I worked alongside at SDU's Department of Molecular Medicine, thank you for welcoming me into your lab and showing me everything I need to know about bones. I acknowledge that it must have taken a lot of patience to teach a mechanical engineer about bone biology, but I'm thankful you did, because none of this would have been possible without your assistance.

I would also like to thank Dr. Bruce Oddson, who answered my numerous questions on statistical analysis, and kindly offered to run analyses for me. Your generous help and guidance has saved me countless hours of work and stress, and has helped me ensure the results are presented accurately.

Lastly, I would like to thank my family for supporting me throughout my studies. Mom and dad, you have always believed in me, and you don't hold back from saying how proud you are of my achievements. I appreciate your attempts to understand my research and what I have been learning as an engineering student, and if you can get through this thesis, you'll have a better idea of what that is. To the both of you and Sam, thank you for providing a safe space for me to vent and take my mind off of research. Your encouragement has allowed me to grow into the person I am today, and I know I will have a successful future with your continued support.

Statement of Authorship

Staining and scanning of the vertebral sections were completed in part by myself, and partly by Kaja Søndergaard Laursen (Laboratory technician, Dept. of Forensic Medicine, Aarhus University, Denmark). Kaja was also responsible for embedding and cutting the vertebrae, as well as developing the staining protocol.

The µCT imaging used to obtain the 3-D architectural parameters of the vertebrae was completed by Jesper Skovhus Thomsen (Associate professor, Department of Biomedicine, Aarhus University, Denmark).

The manual measurement of BSU parameters, the production of graphs, and the linear regression analysis were completed in whole by myself.

The frequency distribution analysis was completed by Dr. Bruce Oddson (Associate Professor, School of Human Kinetics, Laurentian University, Canada), who also provided guidance on statistical analysis techniques.

General supervision and assistance was provided by Dr. Brent Lievers (Associate Professor, Bharti School of Engineering, Laurentian University, Canada), Christina Møller Andreasen (Assistant Professor, Department of Clinical Research, University of Southern Denmark, Denmark), and Thomas Levin Andersen (Associate Professor, Department of Clinical Research, University of Southern Denmark, Denmark).

Contents

List of Figures

List of Tables

Nomenclature

µCT	Micro-computed tomography
BMD	Bone mineral density
BSU	Bone structural unit
#BSU/TP.A	Number of BSU per trabecular profile area
BSU.A	Bone structural unit area
BSU.A.R	Bone structural unit aspect ratio
BSU.Cir	Bone structural unit circularity
BSU.L	Bone structural unit length
BSU.P	Bone structural unit perimeter
BSU.Sol	Bone structural unit solidity
BSU.Th	Bone structural unit thickness
BV/TV	Bone volume per total volume (bone volume fraction)
CL.L	Cement line length
CL.L/TP.A	Cement line length per trabecular profile area
Conn.D	Connectivity density
DA	Degree of anisotropy
MWT	Mean wall thickness
SMI	Structure model index
Tb.N	Trabecular Number
Tb.Sp	Trabecula separation
Tb.Th	Trabecular thickness
TP.A	Trabecular profile area
TP.P	Trabecular profile perimeter

1 Introduction

1.1 Motivation

Age-related bone fractures affect a large portion of the population, and their incidence in industrialized countries is expected to increase due to ageing demographics [1]. Such fractures are costly, not only to those who sustain them, but also to the health care system. An estimated $4.6 billion was spent in 2014 on the hospitalization and treatment of such fractures in Canada [2], and the World Health Organization estimates that there is a 30-40% lifetime fracture risk for those living in developed countries [1].

Skeletal sites with high proportions of cancellous bone such as the spine, the hip, and the wrist are most susceptible to fracture [3]. Also known as spongy or trabecular bone, cancellous bone consists of a complex network of interconnected rods and plates called trabeculae. Cortical (or compact) bone on the other hand, is the denser tissue that forms the shell surrounding cancellous bone [4]. Both are illustrated in Figure 1.1. With age, trabeculae begin to thin or are completely resorbed, causing a decrease in bone mass and leading to osteoporosis [5]. These changes render the bone more fragile and prone to fracture.

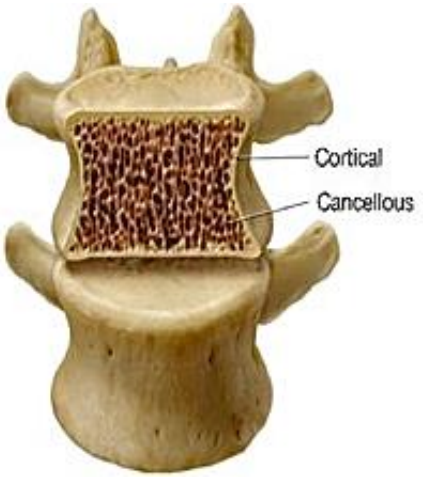

Figure 1.1: A vertebra with a cancellous bone interior surrounded by a cortical shell. Reproduced from [6].

Therefore, predictions of fracture risk are typically made by assessing the quantity of bone (or of bone loss) by means of bone mineral density (BMD) scans. BMD can be measured non-invasively using quantitative computed tomography (QCT) imaging, for example, which provides a 2-D image of the apparent density of cancellous bone (g/cm^2) [7–9]. "Apparent", in this context, indicates that the area used to calculate the density is the one associated with the region of interest, rather than the true area of tissue within that region. BMD tests are used to diagnose osteoporosis, which is defined as a decrease in bone density of more than 2.5 standard deviations below a healthy value [1,10]. This bone quantity measure, however, cannot fully predict bone strength or fracture risk. BMD techniques fail to predict approximately 30% of the variability in bone strength [9], and an observational study on women over the age of 50 who sustained a fracture found that only 31% had osteoporosis [11].

Because BMD alone has proven to be an inadequate predictor of fracture risk, and because BMD is a measure of the *quantity* of bone, more recent studies have focused on the *quality* of bone as well. Quality measures such as the spatial distribution and orientation of the trabecular network (i.e., cancellous architecture) and the material properties of the trabecular tissue have received considerable attention. Specifically, changes in bone quality with age have been used to try and improve predictions of fracture risk.

Bone is a hierarchical material with organization at decreasing length scales (Figure 1.2), and changes in bone quality with age occur at each level. At the larger scale (~10^{-3} m), the thinning of trabeculae in men and the resorption of whole trabeculae in women have been observed with ageing [5,12,13], along with decreased bone volume fraction [5,14,15] and decreased trabecular connectivity [5,16]. At the nano-scale (~ 10^{-9} m), all bone tissue is composed of a mineral-collagen composite [17]. Increases in tissue mineralization [18] and the deterioration of collagen properties [19,20] have been found with ageing, and have been associated with decreased plastic deformation before fracture and increased facilitation of crack propagation [21].

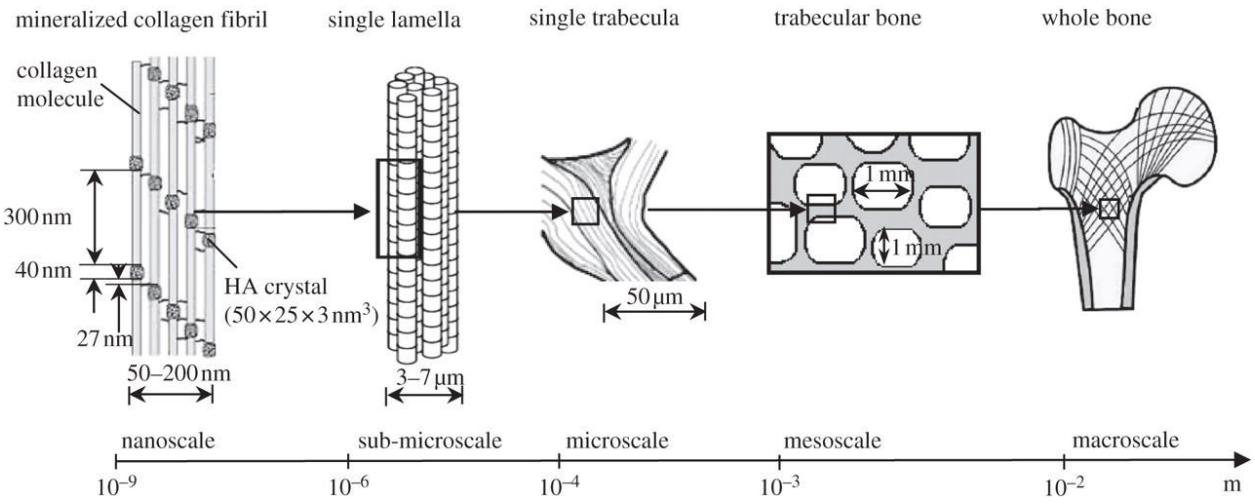

Figure 1.2: Hierarchical structure of bone. Reproduced from [22] with permission from Royal Society (U.K.).

Despite the large body of work that has studied cancellous bone at the architectural and compositional level, much less attention has been given to the intermediate (~10^{-4} m) length scale: trabecular bone structural units (BSU) and the cement line that surrounds them. These BSU, which are often called trabecular packets or hemiosteons, are a result of bone remodeling which occurs throughout our lives. Cells resorb old bone from the surface of trabeculae, while other cells lay new tissue down in its place, resulting in a patchwork of new and old BSU throughout the trabeculae (Figure 1.3). The BSU are separated by a highly mineralized material called cement line.

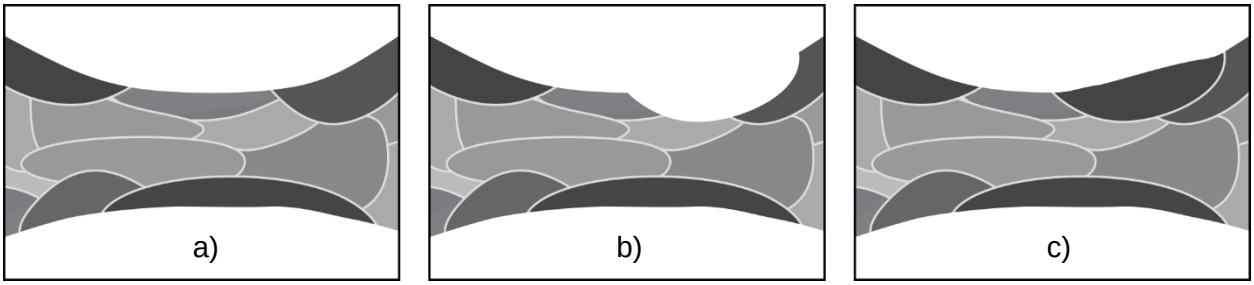

Figure 1.3: a) A trabecula consisting of a patchwork of new and old BSU, separated by cement line (white), b) a portion of bone is resorbed by remodeling cells, c) new bone is laid down in the resorbed portion.

This level in the hierarchical structure has received very little attention, but is expected to contribute to the micromechanical properties of cancellous bone. The cement line that surrounds the BSU is very highly mineralized and low in collagen [23,24]. Because it lacks the toughening

that collagen provides, the brittle cement lines would be expected to fracture more easily and provide preferential paths for microcrack growth. Evidence of this phenomenon has been observed in a study using cyclic four-point bending tests, where the microcracks mostly followed cement lines, and the overall microstructural characteristics of cancellous bone were found to impact the fracture and damage pattern [25]. Because the complicated fracture patterns found in the cancellous bone specimens are determined by the complex nature of their microstructure, any age-related changes to the intricate, mosaic-like population of BSU should have consequences for fracture risk.

A few studies have looked at characterizing BSU, and have found that they become thinner with age and with osteoporosis [26–31]. Unfortunately, because only thickness was measured, it is not clear what other geometric changes may take place. Furthermore, only the surface BSU which were not yet altered by subsequent remodeling were measured, which gives very little information on the overall distribution of the BSU and their relationship to the cement line surrounding them. Still, if there is a significant reduction in the size of BSU with age, as suggested by these earlier studies, it would increase the proportion of cement line contained within trabecula, and could contribute to the increased susceptibility to fracture in the elderly.

Studies on cortical bone have found that the size of osteons (the BSU in cortical bone) affect fracture toughness and ultimate tensile strength of cortical bone, though the results were conflicting [32,33]. Moreover, an increased cement line stiffness, strength, and a lower fracture toughness —which are consistent with a highly mineralized material— have been shown to lead to lower fracture loads and promote crack propagation through osteons in cortical bone [34,35]. Other studies have confirmed high osteonal crack penetration for aged and diseased cortical bone, while also observing that the cracks typically deflected into the cement line in young specimens [36,37]. These studies suggest that crack propagation is influenced by the size and

distribution of the microstructural features of cortical bone, and the same can be expected in cancellous bone.

Some changes in BSU geometry with age have been explored, but many others have yet to be considered. If osteon size, orientation, and distribution —along with the associated changes to the cement line— impact crack formation in cortical bone, a similar relationship would be expected from the BSU in cancellous bone. The first step in clarifying this relationship would be to determine if there are, in fact, any changes in the size and distribution of BSU with age. Based on the results from prior studies [26–30], I hypothesize that BSU do become smaller with age, not only in thickness, but in area and length as well. Decreases in the size of BSU would result in more BSU per unit area, with associated increases in the amount of cement line per unit area. The increased proportion of cement line would likely lead to increased microcrack formation and could contribute to the reduction in bone strength seen with age.

1.2 Objectives and Outline

The goal of this study is to quantify age-related changes in the shape, size, and distribution of trabecular BSU in the lumbar spine. Further, these changes will be assessed as a function of 3-D architectural parameters obtained by μCT as part of a prior study [38]. The 2-D measurements were obtained from high resolution scans of microscope slides of old and young vertebral bone, following a new osteopontin staining process. All the BSU within a region of interest were traced and measured using image analysis software. These digital techniques allow for many geometric measures to be made beyond just the thickness measures obtained in previous studies using manual stereological measurements. Although the material properties will not be measured experimentally in this study, the presence of any changes observed are hypothesized to explain some of the reduction in the mechanical and failure behaviour of cancellous bone observed with age.

This study will provide three main contributions to cancellous bone research:

1. the most complete 2-D morphometric description to date of the most recent BSU is given, where most parameters (e.g. area, length, and shape) are all measured for the first time;
2. all BSU within a region of interest are considered and measured, rather than just the most recent BSU that were considered in prior studies, which gives a more complete description of age-related changes in the microstructure of trabeculae; and,
3. the 2-D morphometric parameters of BSU are, for the first time, compared to 3-D architectural parameters, allowing for a relationship to be made between changes at the BSU level and those at the trabecular architectural level.

The improved characterization of BSU populations, and identifying changes in these populations with age and 3-D architectural parameters, will clarify whether the mechanical consequences of these microstructural changes require further study.

The remaining contents of this thesis are organized as follows:

- Chapter 2: a review of pertinent literature as it relates to the current study;
- Chapter 3: a description of bone specimens, experimental techniques, and statistical analysis methods;
- Chapter 4: the results of the analysis of changes in the shape, size and distribution of trabecular BSU with age and structural parameters; and,
- Chapter 5: a discussion of the work presented, along with a list of conclusions.

2 Literature Review

In order to provide sufficient context to the work presented in this thesis, pertinent literature in the field of cancellous bone has been reviewed and summarized. First, the composition of bone at the macrostructure and microstructure is reviewed with respect to its hierarchical structure. Bones have the ability to adapt to loading due to constant remodeling, which results in a patchwork of old and new bone structural units (BSU); trabecular BSU are the focus of the current study. Changes in remodeling with age lead to increased fracture risk, but current methods of assessing bone cannot sufficiently predict this risk. These methods are reviewed, and characterization of cancellous bone's architectural and tissue properties are explored, with emphasis on the lack of research at the intermediate trabecular BSU level. Finally, difficulties encountered when attempting to predict cancellous bone strength and fracture risk are discussed, and potential factors contributing to bone strength that remain to be studied are identified. It is acknowledged that in order to fully predict bone mechanics, more research needs to be done in the areas of trabecular BSU morphometry and cement line properties in order to create an accurate model of bone representative of its hierarchical structure. By considering this review, and the identified gaps in the literature, the reader should be able to critically evaluate the current study and appreciate its potential contribution to cancellous bone research.

2.1 Bone Overview

Bone is considered to be a calcified tissue, which is a general term used to describe a family of biological structures which may each suit a different purpose. Some examples of calcified tissues include dentin, mineralized tendons, and the cortical and cancellous bone that is seen throughout the bodies of vertebrates [39]. Bones have a hierarchical organization, and all types of bone consist of the same basic building blocks, as depicted in Figure 2.1. The hierarchical structure and the material composition will depend on the role of the bone and the region of the body in which it is present [39]. At the macrostructural level, the function and structure of cortical and

cancellous bone will be considered. The general composition of bones at the microstructural level will also be examined to give insight into its hierarchical structure and to situate the level at which this current study is being conducted.

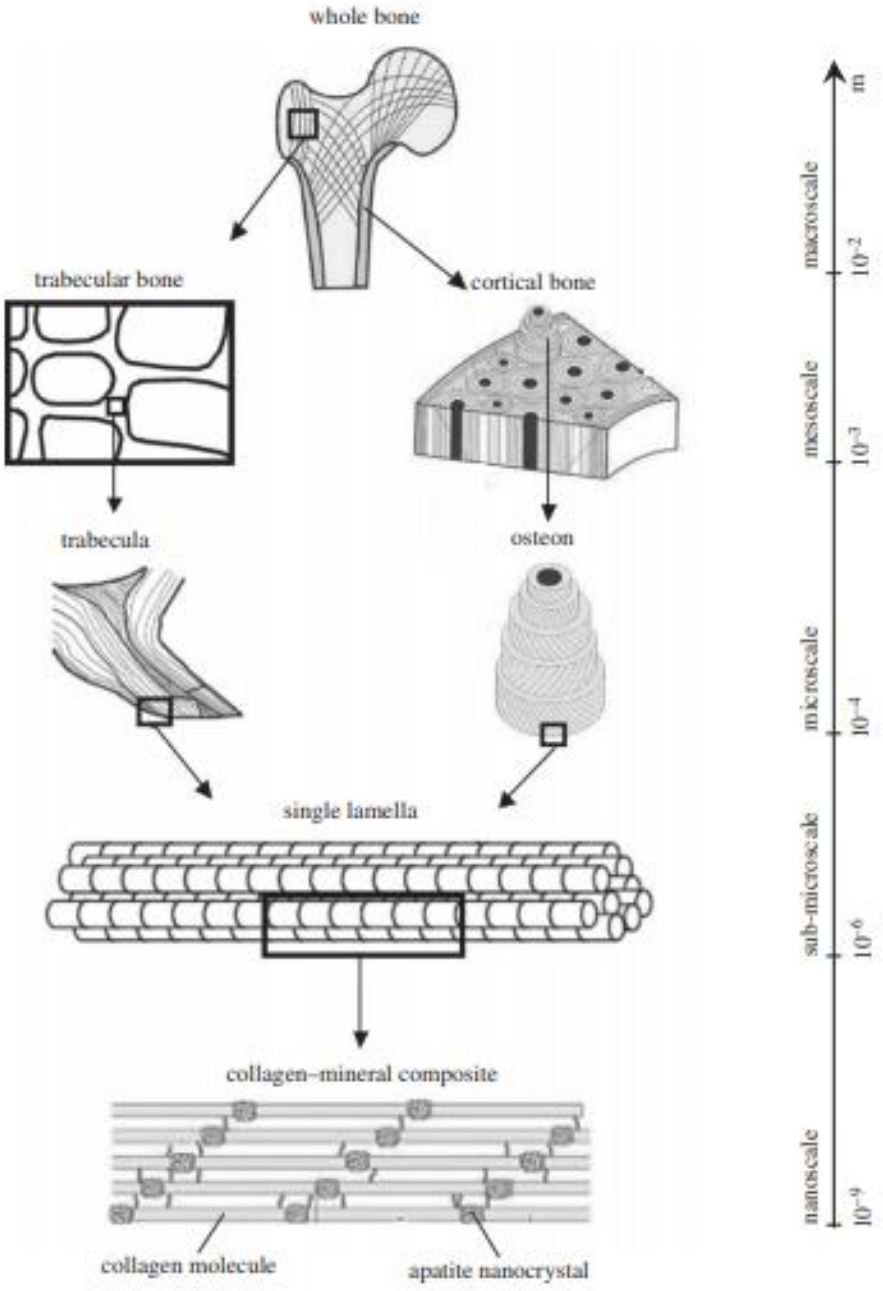

Figure 2.1: Hierarchical structure of bone. Reproduced from [17] with permission from Royal Society (U.K.).

2.1.1 Macrostructure of bone

The difference between cortical and cancellous bone may be seen by the naked eye. Cortical bone is often referred to as compact bone, due to its dense and solid structure [4]. The hard and stiff properties of cortical bone mean it is primarily responsible for providing protection and support of the human skeleton, and accounts for approximately 80% of the human body's skeletal mass [40]. Further investigation into the characterization of cortical bone is outside of the scope of the current study. Instead, specific attention will be given to the structure and characterization of cancellous bone.

Cancellous bone is mainly found in the expanded ends of long bones and in the vertebrae. It accounts for the remaining 20% of the skeletal mass [40]. Cancellous bone, otherwise known as trabecular or spongy bone, is very porous and is formed of a series of interconnecting rods and plates surrounded by marrow [4]. These rods and plates are referred to as trabeculae, and together contribute to an extremely complex architecture. As per the classification system developed by Singh, there are three principle types of cancellous bone: the first is very delicate and made exclusively of fine rods, the second is made of rods and plates that are extremely variable in form, and the third type is composed entirely of plates of varying sizes [41]. The cancellous bone analyzed in the present study is formed of both plates and rods, as seen in Figure 2.2:, thus being classified as Type II as per Singh's system.

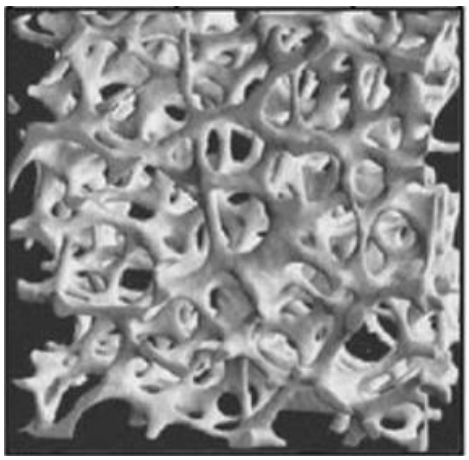

Figure 2.2: Cancellous bone from a vertebral body. Reproduced from [42] with permission from Elsevier.

2.1.2 Hierarchical structure of bone

Roh and colleagues reviewed bone from the sub-nanostructure to the macrostructure, revealing that the most basic building blocks of bone are the mineralized collagen fibrils. These fibrils are approximately 0.5 μm in diameter, and are formed of mineral crystals embedded in an organic matrix consisting of collagen molecules and non-collagenous proteins such as osteopontin, a phosphoprotein [43]. The mineral portion, which accounts for around 65% of the bone's composition [40], is responsible for providing bone its stiffness, while the collagen provides toughness [44]. The properties of bone depend on both these constituents, which are present in different proportions depending on the type of bone, the age of the individual, and the presence of disease [18–20,45]. Collagen fibrils assemble to create collagen fibers, which then form planar sheets that typically stack together in a plywood-like arrangement with alternating orientations. These sheets are called lamellae, and are 3–7 μm thick [43]. In some cases, the lamellar structures can be observed under polarized light (Figure 2.3 a).

The structural units created by lamellae present differently depending on the type of bone tissue. In cortical bone, the lamellae are wrapped concentrically around a central canal to form osteons of 200–250 μm in diameter (Figure 2.3 a). In cancellous bone, they are aligned tangential to the outer surface of the bone without forming osteons, but instead creating crescent-shaped hemiosteons (Figure 2.3 b). These trabecular bone structural units (BSU) are the focus of the present study.

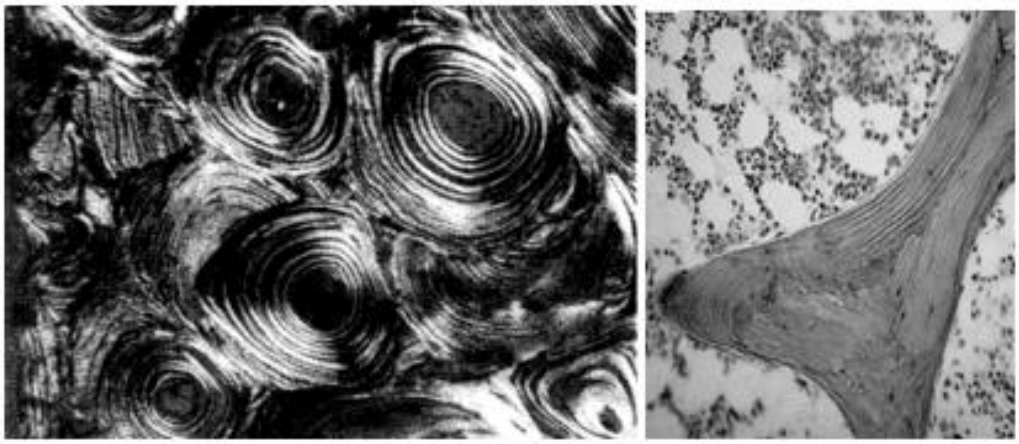

Figure 2.3: Lamellar structure of a) cortical bone osteons and b) cancellous bone BSU seen under polarized light. Adapted from [46] which was itself modified from [47]. Used with permission from Elsevier.

The reader should refer back to Figure 2.1 for a clear depiction of the hierarchical structure reviewed in this section.

2.1.3 Role and functional adaptation of cancellous bone

The particular role of cancellous bone is dependent on the region of the body in which it is located. In short bones like the vertebrae, cancellous bone is enclosed in a thin shell of compact bone. The loads in these bones are mainly compressive, where the cortical shell provides a flat surface to evenly distribute the load born by the cancellous material [4]. Considering the role of the skeletal system is to provide support and protection of the body, it is intuitive that the primary requirement of bone is for it to be stiff. Yet, cancellous bone is found to have significantly lower stiffness and strength than cortical bone, though there is some variability in the values due to the complex architecture of the material [4]. As natural selection favors efficiency, the design of bones is such that the required stiffness is provided with minimal mass, material, and energy costs. An increase in mass would require higher levels of energy to be spent on locomotion, while large amounts of material and the required energy to form it would have a high metabolic expense. As such, the porous nature of cancellous bone makes it an efficient structure to reduce the weight and material necessary to provide the required stiffness in whole bones [4].

With efficiency in mind, bones are able to adapt to their environmental and mechanical demands. An example of this is the loss of bone mass observed in astronauts who undergo long periods of weightlessness where the skeletal system experiences significantly lower gravitational and muscular forces [48]. Similarly, a study investigating the effects of sport-specific strains on the skeletal system found that the bones in the forearms and hands of the stroke arm of professional tennis players have an increased diameter, density, and length compared to the contralateral arm [49]. The functional adaptation of bone allows for an optimal design for the skeleton's functional requirements. This phenomenon is possible due to the constant remodeling that bone undergoes.

2.2 Remodeling

Our skeletons continuously undergo remodeling throughout our lives, where portions of old bone tissue are destroyed and new tissue is deposited in its place. This process creates a patchwork of new and old bone tissue which promotes skeletal health. The remodeling process can take place for a number of reasons, such as to replace damaged tissue, to adapt to current loading conditions, or to reclaim the resources in overdeveloped regions based on the current metabolic needs [4]. Different bones undergo remodeling at different rates. The potential signals for initiating remodeling, and the ways in which they are communicated, are not yet fully understood and are outside the scope of this research. The concept of remodeling will be introduced by first giving an overview on the cells responsible for remodeling, and then discussing the resulting structures they create. The remodeling process is roughly the same in both cortical and cancellous bone, with the only difference being the location of remodeling events and the shape of the newly formed structures. The following sections will thus focus on the remodeling process as it relates to cancellous bone specifically.

2.2.1 Remodeling cells

The sequence of activities contributing to bone remodeling include bone resorption, deposition, and mineralization. This process is possible due to the contribution of two main cells: osteoclasts and osteoblasts. First, the large, multinucleated osteoclasts resorb a portion of tissue at the trabecula's surface by dissolving the bone mineral while enzymes digest the organic macromolecules [50]. Next, osteoblasts deposit new bone. In this step, osteoblasts secrete the necessary macromolecules to lay down an organic matrix called osteoid. They regulate the assembly of the major structural elements of osteoid, and facilitate the mineral deposition on to the osteoid by means of mineral salt precipitation [50]. There is an intermediate step between the bone resorption and formation which is called the reversal stage, a process which lasts 1-2 weeks [40]. Delaisse has recently reviewed the reversal phase in detail, recognizing that osteoclast leave behind some mononuclear cells of unknown origin that somehow allow for the coupling of bone resorption and formation in space and time [51]. After the bone has been deposited, inactive osteoblasts called lining cells coat the surface of the deposited bone, and have the potential to become active osteoblasts. Some bone cells become buried within the deposited bone and are called osteocytes [52].

A review by Parfitt depicts the stages of cancellous bone remodeling [53]. The resorption step creates a cavity through erosion of bone perpendicular to the trabecula's surface. This cavity is then refilled with new bone in the deposition phase. However, the bone does not necessarily have to be resorbed before being modeled over, and new tissue may be added at the surface of existing bone. The sequence of activities outlined above is depicted in the simplified schematic of Figure 2.4, and culminates in the creation of a new bone structural unit, or in the specific case of cancellous bone, a hemiosteon.

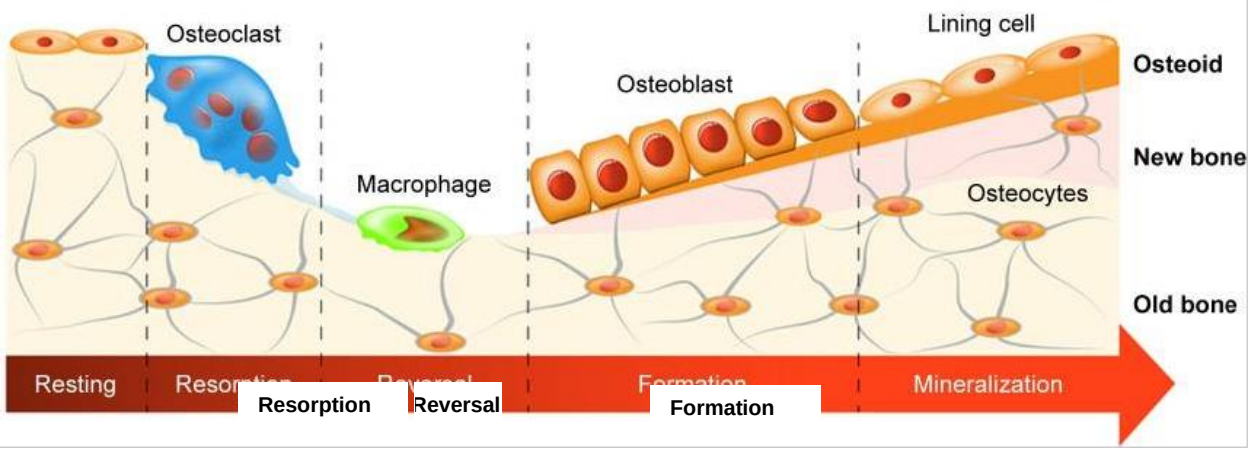

Figure 2.4: Schematic of bone remodeling process. Creative Commons (CC BY-NC 3.0) image reproduced with permission from [54]

2.2.2 Hemiosteons

The remodeling process results in a patchwork of new and old hemiosteons of varying shapes and sizes. In general, hemiosteons, which will henceforth be referred to simply as BSU, are irregular and elongated in their 3-D shape. In 2-D, newly remodeled BSU in the iliac crest have been reported to be approximately 585 µm in length [55], and 41–58 µm in thickness [30], though these values are highly variable and are likely impacted by age, sex, and skeletal site.

As briefly discussed, the BSU undergo mineralization when they are laid down, but this mineralization does not end once the BSU is completed. Instead, the level of mineralization increases with time, meaning that not only does trabecular bone consist of BSU of varying shapes and sizes, but also of varying degrees of mineralization. Up to 70% of the initial mineralization is completed in the first few days of bone formation, while the remaining 30% is accomplished over the next several years [44]. As such, older BSU at the interior regions of trabeculae have higher degrees of mineralization, while those that are newly remodeled at the surface are less mineralized. This may be observed by use of quantitative backscattered electron imaging [56], as examined in a study by Fratzl et. al. [44], where the greyscale colours of BSU are indicative of their mineral content (Figure 2.5). The higher mineral content in the interior BSU, and the lower

mineral content in the newly remodeled surface BSU should be noted. Because the level of mineralization is related to the bone's stiffness and hardness, the variability in the degree of mineralization means the trabeculae also have tissue-level heterogeneity in mechanical properties [57].

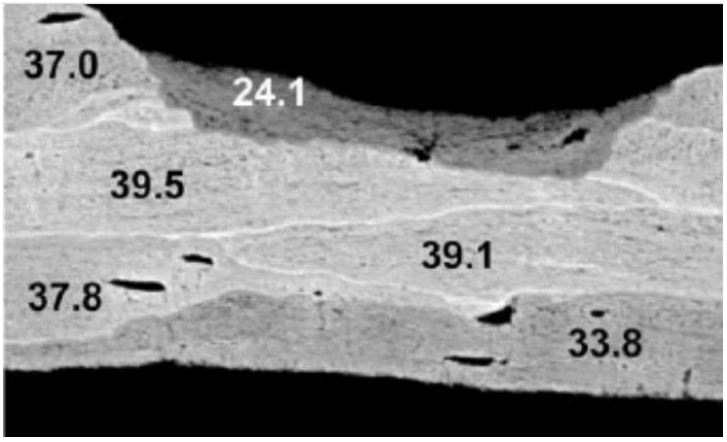

Figure 2.5: The mineral content of trabecular bone BSU. Reproduced from [44] with permission from Royal Society of Chemistry.

2.2.3 Cement line

Surrounding the trabecular BSU are thin layers of material called cement lines. These may be scalloped and irregular, which indicates osteoclastic resorption took place, or they may be smooth, thick, and well-defined, which indicates that new tissue was deposited without prior resorption (Figure 2.6).

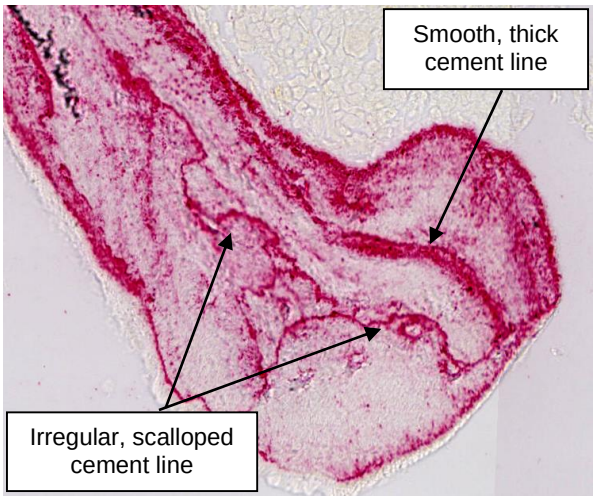

Figure 2.6: Pink-stained cement lines separating the BSU.

Very little is known about the exact properties and functions of the cement line, particularly for cement line in trabecular bone, but it seems to have a different material composition than the BSU. Like BSU, there is a mineral and an organic component to the cement line, but the quantities differ from those seen in regular bone. A study by Smith, who refers to the cement lines as "reversal lines", found through microincineration that the cement lines surrounding osteons in cortical bone had less carbon residue, inferring that cement lines have a very high ratio of mineral to organic material compared to the adjacent osteons [23]. Similarly, a study using quantitative backscattered electron imaging found that the cement lines were visualized as bright lines, which indicates a high atomic number, and may represent hypermineralization or collagen deficiency relative to the surrounding tissue [24].

The cement line may play an important role in cancellous bone's fracture behaviour. A few studies on cortical bone have found that having a stiff and brittle cement line, consistent with a highly mineralized material, reduces crack initiation load and promotes crack penetration directly through the osteons [34,35]. In cancellous bone, Choi and Goldstein found that rectangular beams of cancellous bone tissue that underwent cyclic bending had more complicated fracture patterns

that were mostly associated with cement line, compared with the more direct transverse cracks seen in cortical bone (Figure 2.7) [25].

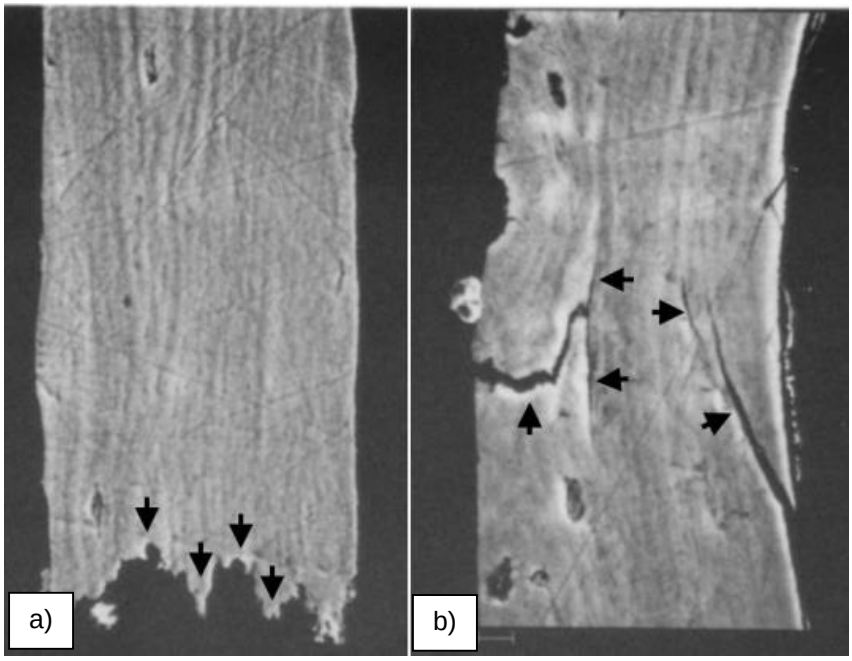

Figure 2.7: Backscattered electron images of the microcrack patterns on ~120 μm wide machined beams of a) cortical bone, and b) cancellous bone, following cyclic bending. Cortical bone experienced transverse cracking, while cancellous bone experienced oblique cracking along the cement lines, as indicated by the arrows. Reproduced from [25] with permission from Elsevier.

A potentially important component of the cement line is osteopontin, and its implications are discussed in a review by McKee and Nanci. Osteopontin is an acidic phosphorylated protein secreted by osteoblasts during the remodeling phase and concentrated in the cement lines. This protein contains a distinctive 3-D structure that promotes cell adhesion, and *in vitro* studies have demonstrated its ability to bind to mineral and inhibit crystal growth [58]. The high concentration of osteopontin in the cement lines could mean that one of the roles of cement line is to act as an adhesive that binds the BSU together. In this study, osteopontin-specific staining will be used to identify cement line so that the shape of the BSU can be measured.

2.3 Age-related fractures

Changes with age in the remodeling process result in a net bone loss, which can lead to common diseases like osteoporosis, and is accompanied by a reduction in strength and an increase in

fracture risk. Additionally, an accumulation of microdamage decreases cancellous bone's resistance to fracture, causing fractures to occur after only minor trauma events in the elderly [59–61]. Common sites for these fractures are the vertebrae, wrists, and hips, and the World Health Organization estimates that in developed countries there is a lifetime fracture risk of 30–40% in one of these anatomical locations [1]. Fractures carry a high burden, both to the patient and to health care resources. The physical and mental quality of life of patients who sustain age-related fractures is reduced [62], while the annual costs of hospitalization and treatment of osteoporotic fractures were $4.6 billion in Canada as of 2014 [2]. These numbers are certainly higher when considering age-related fractures that were not associated with osteoporosis, and are expected to increase by more than threefold over the next 50 years due to the ageing population [1].

2.3.1 Predictors of fracture risk

Bone mineral density (BMD) is the standard test used to determine the quantity of bone in a 2-D region of interest (g/cm^2) [7]. Some methods of obtaining BMD measures *in vivo* include quantitative computed tomography (QCT), dual photon absorptiometry (DPA), and dual energy X-ray absorptiometry (DXA). These techniques are highly correlated with bone strength and, because they are non-invasive, are thus often used in predicting fracture risk in clinical settings [8]. Unfortunately, these techniques still fail to explain approximately 30% of the variability in bone strength, as they only provide 2-D images of apparent density [9]. A more accurate prediction of vertebral bone strength is obtained by characterizing and testing iliac crest bone biopsies; however, this method is very invasive and cannot be performed more than twice on one individual [8].

In general, women are more prone to fracture than men. Though bone loss begins gradually in both sexes after approximately 25–30 years, there is a five- to ten-year window of increased bone loss in postmenopausal women [63]. As reviewed by Chappard et al., an estrogenic deficiency brought on by menopause leads to a stimulation in osteoclastic activity, and

the osteoclast life span is increased. Consequently, there is a net bone loss, with an increased occurrence of trabecular perforation and erosion of whole trabeculae [64]. This phenomenon explains why women over 50 have four times higher rates of osteoporosis and two times higher rates of osteopenia than men [10]. Other clinical risk factors for bone loss as outlined by the World Health Organization include low body mass index (BMI), glucocorticoid exposure, a parental history of hip fracture, smoking, excessive intake of alcohol, and rheumatoid arthritis [1].

2.3.2 Osteoporosis

An obvious and very common disease related to fractures is osteoporosis. This disease is defined by a decrease in bone density that results in micro-architectural deterioration [10], as may be observed in Figure 2.8. As discussed above, BMD tests are a method of predicting fracture risk and are used to diagnose osteoporosis. According to the World Health Organization, osteoporosis is defined by a BMD that is 2.5 standard deviations (SD) or more below the average value for young, healthy women, and osteopenia is described as low bone mass with a BMD score that is 1 to 2.5 SD below the mean [1].

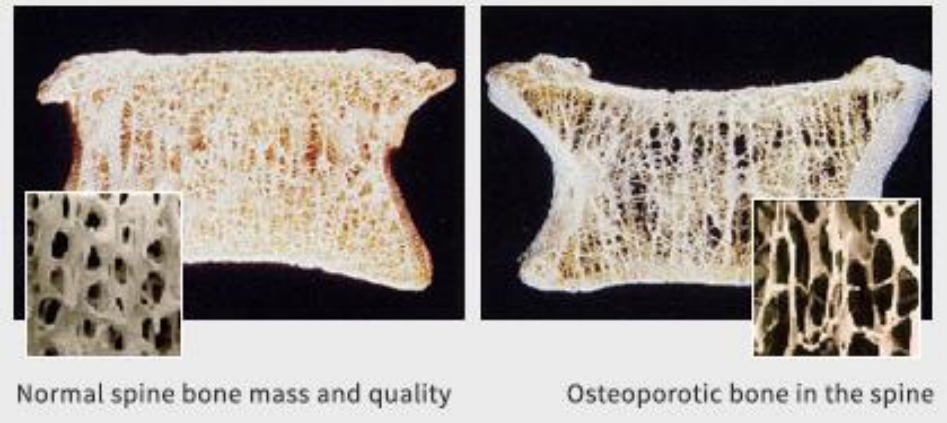

Figure 2.8: Comparison between a healthy vertebra (left) and an osteoporotic vertebra (right). Reproduced from [65].

Still, a diagnosis of osteoporosis is not necessarily optimal for detecting individuals at high risk of fracture. Although fracture risk is very high in those diagnosed with osteoporosis by means of BMD tests, those who have a normal BMD can still be at risk; in fact, those with normal BMD

account for over 1/3 of all age-related fractures [1]. An observational study at the Murnau Trauma Center in Germany looked at characterizing the fractures of women who reported to the Center with a fresh fracture from either minor or moderate trauma. Of the 233 patients (aged 50-94) studied, 31% had osteoporosis, 34% had osteopenia, and 36% had normal bone density. Only about one third of minor trauma fractures occurred in women diagnosed with osteoporosis [11]. This study further suggests that the diagnosis of osteoporosis by BMD alone is insufficient to predict the risk of fracture in the ageing population. Research efforts have thus begun to focus on other characteristics of trabecular bone to better understand decreased strength and increased fracture risk with age.

2.4 Measures of age-related changes

As the *quantity* of bone is not an adequate parameter to determine fracture risk, more recent research has focused on assessing the *quality* of bone. At the larger scale, changes in the trabecular architecture with age have been thoroughly examined and standard parameter measurements have been established. At the tissue level, the changes in the quality of the collagen fiber matrix have also been studied; however, little attention has been given to the changes in the trabecular BSU at the intermediate scale.

2.4.1 Measures of trabecular architecture

Trabecular architecture was initially characterized based on 2-D histological analysis on thin sections of bone, and Parfitt et al. devised methods for examining these structural changes. Their methods included measuring the trabecular bone area as a fraction of total trabecular tissue area, as well of the perimeter of the marrow-bone interface. Using principles of stereology and the parallel-plate method which assumed idealized structures, they were able to derive 3-D quantities such as fraction of bone volume per total volume, trabecular thickness, and trabecular separation from these 2-D measures [66]. Now, direct 3-D architectural characterization is possible with the

use of micro-CT imaging and provides more accurate results [67]. The most commonly used indices, and the changes in their values with age, are described below.

2.4.1.1 Bone Volume Fraction

Bone volume fraction (BV/TV) is the ratio of bone tissue volume (BV) to total volume (TV) of the region analysed [67]. One review noted that BV/TV decreased by 22–24% in the lumbar vertebrae and 18–22% in the femoral neck between the ages of 60 and 90 years [5]. These data are supported by other studies on the distal radius, tibia, femur, and lumbar vertebra [14,15,68,69] with similar findings. In an attempt to quantify the effects of the reduction in BV/TV seen in ageing, Barak and Black printed and compared 3-D models of healthy trabecular bone and the same model after bone loss. They found that an 8% reduction in BV/TV resulted in a 24% reduction in structural strength and a 17% reduction in stiffness [70], indicating the large dependence of mechanical properties on the quantity of bone as determined by bone volume fraction.

2.4.1.2 Trabecular Thickness

Mean trabecular thickness (Tb.Th) of cancellous bone is defined in 3-D by the arithmetic mean value of the local thicknesses, taken by fitting maximum spheres to every point in the trabecular structure [71], as depicted in Figure 2.9 a). There is, however, controversy surrounding changes in trabecular thickness with age. While some studies found 10–24% age-related decreases in trabecular thickness in the proximal tibia, distal radius, and the femur [12,13,68,69,72], others found no significant changes in the vertebra [16,38]. One study found a significant decrease in Tb.Th of the distal radius with age in men (16%), while the decrease in women (2%) was not significant [14]. Interestingly, Thomsen and colleagues found that age-related thinning of horizontal trabeculae in women was accompanied by compensatory thickening of vertical trabeculae [73], which may be why the overall trabecular thickness in women does not always decrease significantly [38]. This metric has been demonstrated to play an important role in the prediction of the primary Young's modulus and shear modulus in the lumbar spine [74].

2.4.1.3 Trabecular Separation

Similar to trabecular thickness, mean trabecular separation (Tb.Sp) is measured using the diameter of the maximum sphere filling the marrow spaces [71], as depicted in Figure 2.9 b).

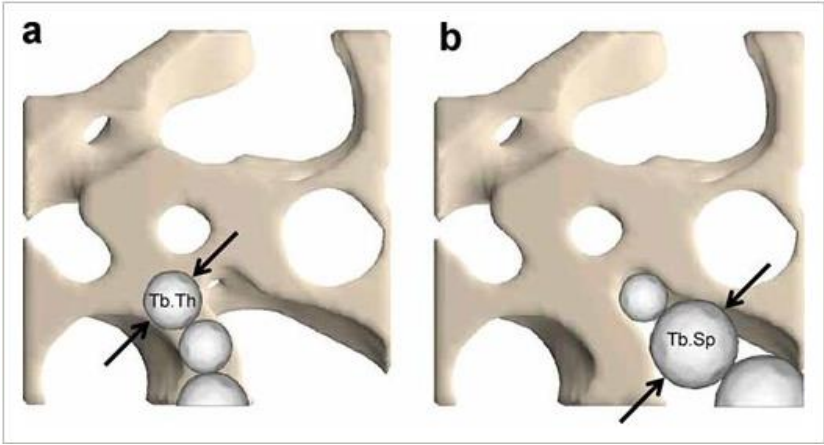

Figure 2.9: Representation of the 3-D methods used for calculating a) trabecular thickness (Tb.Th) and b) trabecular spacing (Tb.Sp.). Reproduced from [75] with permission from John Willey and Sons.

Trabecular separation has been shown to increase 15–24% with ageing in the lumbar vertebra, radius and femur [12,16,69]; however, these changes are not equal in women and men. One study on the radius found a 24% increase in trabecular separation between 20 and 90 years of age in women, but no significant change in men [69], and while not statistically significant, another found the age-related increase was 12% more in women compared to men [14]. The shear and primary Young's moduli were found to be significantly impacted by the increased trabecular spacing in the femoral head.

2.4.1.4 Trabecular Number

Trabecular number (Tb.N) is the average number of trabeculae per unit length (1/mm). It is calculated as the inverse of the mean distance between the central-axes of each trabecular structure [75], found using Euclidean distance maps [76]. Significant reductions in trabecular number of 9–19% were found with age in the proximal femur and the vertebra [12,16], but not in the proximal tibia [13]. Macdonald and colleagues found that, though not statistically significant, the age-related decrease in trabecular number in the radius was 8% greater in women than in

men [14], while Khosla et al. found that the decrease was only significant in women [69]. This gender difference, supported by findings of no significant difference in trabecular thickness in women [14,38] and larger reductions in Tb.Sp in women [14,69] suggests that, contrary to men, bone loss in women is primarily due to the loss of whole trabeculae, rather than trabecular thinning [5,69]. A 10% reduction in the number of trabeculae was found to reduce the strength and elastic modulus of cancellous bone two to five times more than the same loss of bone volume through uniform trabecular thinning [77].

2.4.1.5 Trabecular Connectivity

Trabecular connectivity, also known as connectivity density (Conn.D), characterizes the number of trabecular connections per unit volume ($1/mm^3$) [78]. This is calculated using a complex equation which considers the number of objects, the number of marrow cavities fully surrounded by bone, and the number of connections that must be broken to split the structure into two parts, and dividing this by the total bone/marrow volume [75]. With age, reductions in Conn.D were found in the lumbar vertebra [16] and the femoral neck [72]. As described in Section 2.1.1, cancellous bone is composed of a series of interconnected plates and rods; as the number of plates and rods decreases, the number of connections in the structure also decreases. This change means that Conn.D is highly correlated to Tb.N, and expected to similarly impact the mechanical properties of cancellous bone.

2.4.1.6 Structure Model Index

With the deterioration of cancellous bone structure with age, studies have observed a conversion from plate-like to more rod-like trabeculae in various anatomical locations. However, the classification of a trabecula as plate-like or rod-like is subjective. Because of this, Hildebrand and Ruegsegger developed a morphometric parameter to quantify these architectural changes called the Structure Model Index (SMI), which is determined by a mathematical model relating the trabecular volume and surface to a number of form-dependent measures of the structure. The SMI value of an ideal plate is 0, while that of an ideal cylindrical rod structure is 3 [79]. This index

allows for the objective determination of changes in the plate-rod composition of trabecular bone with age, sex, or across skeletal sites. SMI has been widely used since its creation, and the cancellous bone in the human proximal tibia [5,13], lumbar vertebrae [16], femoral neck [72] and calcaneal bone [7] are shown to demonstrate higher SMI values with increasing age, meaning they become more rod-like.

It should be noted, however, that a more recent study has found that this method of trabecular structure classification is flawed. SMI is strongly related to BV/TV, and has the underlying assumption that all trabecular surfaces are convex, whereas a high proportion of the surfaces of the complicated connections within the trabecula are concave. This assumption may lead to deceptively higher SMI values, and the apparent shift from plate-like to rod-like trabeculae with age could be explained by the reduction in bone volume and an increase in concave trabecular surfaces. It was thus suggested that SMI results reported in literature should be treated with suspicion [80].

In sum, a number of architectural parameters are used to characterize trabecular architecture and the changes seen in ageing. With their use, it was determined that the primary modes of bone loss in women are the loss of whole trabeculae and an increase in trabecular spacing, whereas men experience bone loss by means of trabecular thinning, which results in a decrease in trabecular thickness, but the number of trabeculae remains unchanged [5]. When considering a combination of these structural parameters, Ulrich and colleagues found that between 81% and 92% of the bone's elastic constants can be predicted, a significant increase from the 53% prediction using BV/TV alone [74].

2.4.2 Tissue-level changes

Age-related changes at the tissue level have also been investigated. The most widely examined tissue-level parameters are the degree of mineralization and the quality of the organic matrix. The mechanical properties of bone depend on both of these components: the mineralized portion

provides stiffness, while the organic matrix (mainly composed of type I collagen) is softer and provides toughness [44]. Together, and in the right proportions, they form bone with both high stiffness and toughness.

As mentioned earlier (Section 2.2.2), the level of mineralization in bone can be determined by means of quantitative backscattered electron imaging. Alternatively, it may be found by the density fractionization technique, where bone is ground, sieved to a small particle size, and centrifuged in organic solvents to separate it by density. The higher the density, the higher the mineral content [18]. Ciarelli and colleagues studied the levels of mineralization of the iliac crest in females with and without fracture and found that, although both populations had the same mean mineralization values, those who sustained fractures had completely different mineralization distribution than their healthy controls, supporting the idea that areas of very high and very low mineralization contribute to fracture [45]. On the other hand, Grynpas found that bone hypermineralizes with ageing [18]. Currey et al. associate the increase in the mineralization in bone with the decreased plastic deformation before fracture and facilitation of crack propagation in ageing [21]. Changes in mineralization, combined with studies supporting deteriorating collagen properties with age [19,20] may help explain why bones often fracture after very little trauma in the elderly.

2.4.3 Changes in trabecular BSU

Although significant research has been done at the whole trabecula and tissue level of cancellous bone, the BSU level has largely been ignored. This intermediate level received some limited attention in the 1970s and 80s, but has been abandoned. The difficulty and tediousness of measuring the BSU with the technology of the era is likely to blame.

One very well-known paper in the field, published by Lips and colleagues in 1978, examined how the mean wall thickness (MWT) of trabecular BSU changes with age. Thin sections of the iliac crest bone samples from 36 men and women who died suddenly between the ages of

18 and 90 were stained and observed under polarized light. The thickness was measured on 30 BSU per patient, and calculated as the average of 4 equidistant measurements between the cement line and the marrow, as depicted in Figure 2.10. A very significant negative correlation was found between the MWT and age in both males and females, which the authors attributed to a decrease in bone formation with ageing that can partly explain senile osteopenia [30]. Similar results were found in subsequent studies using comparable stereological techniques [26,29].

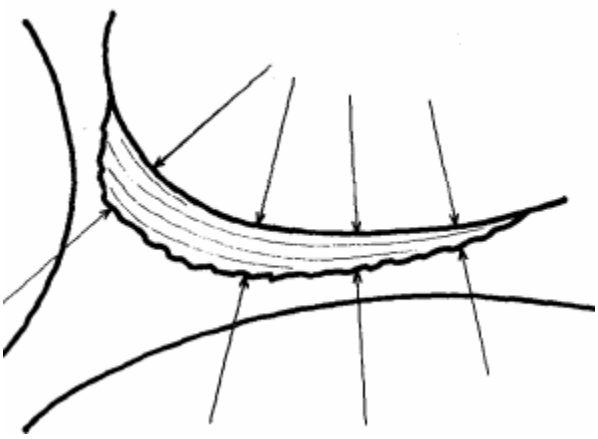

Figure 2.10: Measurements of mean wall thickness. Reproduced from [30] with permission from Springer Nature.

The effects of disease and drugs on BSU thickness have also been explored. Idiopathic osteoporosis caused a reduction in MWT [27], while patients suffering from hypothyroidism (who had elevated levels of serum thyroid stimulating hormone and low serum thyroxine) were found to have an increased MWT [81]. Patients with osteoporosis induced by corticosteroids were also found to have reduced MWT compared to their age- and sex-matched controls [28].

Of the studies that characterized BSU, most relied exclusively on MWT. One notable exception is a conference paper by Ohno and colleagues where area and perimeter were also reported [82]. Unfortunately, the methods section is only four sentences long so the techniques for measuring perimeter and area are not described. They did not measure MWT directly, as per most previous studies, but instead estimated it by dividing BSU area by half the perimeter. This

estimation approach seems flawed due to the frequent crescent shape of BSU, and the overall lack of methodological detail makes it hard to evaluate the reliability of the results. Nevertheless, my own analysis of their reported data for mean values measured from the iliac crest of 98 Japanese women (12–77y) indicate significant reductions in thickness, area, and perimeter with age.

These limited findings, however, are more indicative of how bone remodeling is affected by age, disease, and drugs, rather than how the distribution, shape and size of BSU change with these factors. The MWT was measured on only the newly remodeled surface BSU that were not yet altered by the remodeling process, so very little is still known on the overall distribution of BSU and their relationship to the cement line that surrounds them; however, changes at the BSU level could have implications for the mechanical and fracture behaviour of bone.

These microstructural effects have been investigated using numerical modelling. For example, Hammond and colleagues used μCT imaging to a create an extended finite element model of a cancellous core from the distal femur, and accounted for heterogeneity in the mineralisation of the BSU throughout the trabeculae. They found that anisotropy and heterogeneity of BSU tissue contribute significantly to increased tissue toughness and resistance to microcrack formation in cancellous bone [83]. Additionally, in cortical bone studies, the size of osteons and the number of osteons per unit area was found to alter the crack initiation toughness and ultimate tensile strength, which was attributed to changes in the proportions of cement line that was associated with changes in osteon size and distribution [32,33].

In order to fully understand how each of these hierarchical levels contribute to the mechanical properties of trabecular bone, more research needs to be done at the level of trabecular BSU and cement line.

2.5 Literature review summary

The literature relating to cancellous bone and the known factors influencing its deteriorating mechanical properties with age have been reviewed. There has been significant progress in the last few decades in establishing trabecular architectural parameters to help predict fracture risk, but they still cannot fully explain the variation in bone strength observed with ageing. Based on the gaps in the literature that have been identified, it is suggested that more attention be given to the intermediate level of cancellous bone to better account for changes at this level of its hierarchical structure.

The morphometry of trabecular BSU has not been thoroughly investigated in any prior study, and their potential implication in the fracture mechanics of cancellous bone remains unknown. Any changes in the shape, size, and distribution of trabecular BSU, along with their relationship to the surrounding cement line, could be responsible for variations in the mechanical properties of cancellous bone that remain unaccounted for. Taking these age-related changes into consideration and gaining better insight into the cement line properties could allow for better prediction of fracture risk in the elderly. Therefore, the goal of the current research is to address the first of these needs by characterizing the morphometry of trabecular BSU in the lumbar vertebra.

3 Materials and Methods

3.1 Specimen selection

The second lumbar vertebra (L2) of 8 young women (aged 18.53-37.61, mean 28.45) and 8 old women (aged 69.08-96.39, mean 79.33) were obtained from collaborators in Denmark. Because the specimens were collected as part of an earlier study [84], the approval of Laurentian's Research Ethics Board (REB) was not required. The specimens represented a subset, selected based on age, from among the 41 L2 vertebrae used in the prior study that were subjected to non-destructive analyses and 3-D μCT imaging [38,73]. The 3-D architectural parameter obtained by μCT for the 16 specimens were provided for use in the current study, and included bone volume fraction (BV/TV), structure model index (SMI), connectivity density (Conn. D.), trabecular number (Tb.N), trabecular separation (Tb. Sp), and trabecular thickness (Tb. Th). These parameters were defined in section 2.4.1, and the values for each of the 16 specimens are presented in Table 3-1. Only one-half of each vertebra was available for the current study, as the other half was used in destructive testing [84–88]. The vertebrae were halved along the medial plane (Figure 3.1 a) using a diamond parallel precision saw (Exakt Apparatebau; Otto Herrmann; Norderstedt, Germany). Due to left-right symmetry in the vertebral bodies, this does not affect the analysis results.

Table 3-1: Subject age, and their values for vertebral 3-D architectural parameters obtained by μCT from [73].

	Age (years)	BV/TV (%)	SMI	Conn. D (mm^{-3})	Tb. N	Tb. Th (μm)	Tb. Sp (μm)
Young	**18.5**	14.04	0.80	4.31	1.15	135	0.84
	21.4	15.01	0.78	4.46	1.22	131	0.78
	21.7	16.20	0.77	5.83	1.25	134	0.77
	26.2	11.86	1.29	7.36	1.27	107	0.75
	30.2	11.95	1.37	5.87	1.13	122	0.85
	35.7	12.52	1.20	7.02	1.19	119	0.80
	36.2	15.03	0.72	6.47	1.18	118	0.82
	37.6	15.60	0.62	4.63	1.08	143	0.89
Old	**69.1**	5.43	2.36	3.58	0.95	107	1.01
	71.6	7.88	1.89	1.66	0.75	176	1.31
	73.5	6.85	2.47	1.71	0.83	179	1.19
	77.3	6.95	1.79	2.77	0.93	115	1.04
	78.0	7.47	1.39	3.45	0.84	123	1.18
	83.0	5.43	1.97	2.72	0.90	110	1.09
	85.8	7.42	1.90	8.56	1.11	104	0.89
	96.4	8.24	1.27	3.30	0.75	149	1.35

As documented in an earlier study using these specimens [73], the individuals were Caucasian, and were considered in reasonably good health prior to death. Individuals with identified vertebral fractures were excluded from the study. Further investigation into the medical records allowed for the exclusion of individuals with cancer discovered at autopsy, metabolic disease, severe liver or kidney disease, the use of medication affecting bone metabolism, and those who had a period of more than two weeks of immobilization prior to death. Only the vertebrae of women were considered for this study, as prior research has demonstrated that the modes of bone loss differ in women and in men. Vertically oriented trabeculae are lost more

quickly in women compared to men [73], and decreases in bone volume are mainly attributed to trabecular thinning in men, but due to the loss of whole trabecula in women [5,12,13]. Because women undergo increased rates of bone remodeling and bone loss during menopause [63], the age of the specimens in the “young” and “old” groups were chosen to be well below, and well above, the age of menopause, respectively.

3.2 Specimen Preparation

As described by Thomsen et al. [73], the undecalcified specimens were cut in 9 mm thick frontal mediolateral sections (Figure 3.1) and embedded in methyl methacrylate (MMA) (Technovit 9100; Heraeus Kulzer; Wehrheim/Ts., Germany), a technique that prevents the vertebrae from changing or degrading over time [89]. The tissue blocks were then trimmed using a diamond saw to remove any excess MMA in order to facilitate the µCT scanning.

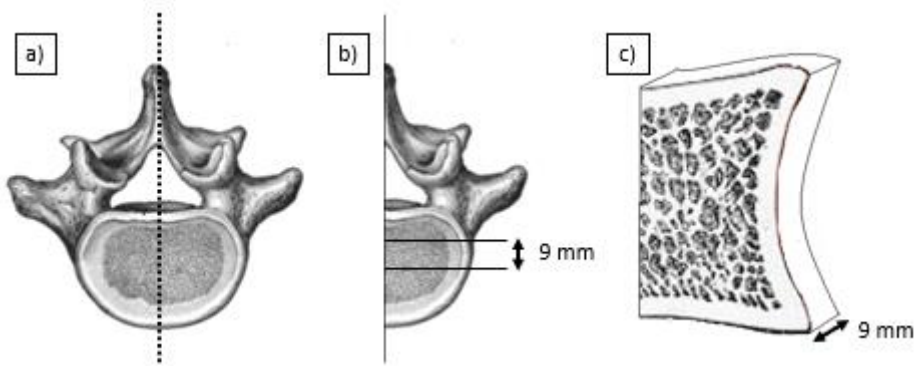

Figure 3.1: Schematic of the vertebrae provided for this study: a) a transverse view of a lumbar vertebra and the median plane along which the vertebrae were halved, b) a 9 mm thick frontal section was cut from the middle of each of the halved vertebrae, and c) an orthographic projection of the 9 mm thick section which we were provided for this study. Adapted from [90,91].

In this study, the 9 mm thick vertebral sections were re-embedded with MMA to increase their size enough to allow them to be properly gripped by the fixtures of the Leica SM 2500 microtome. The embedded vertebrae were then sectioned at a thickness of 7 µm. Each thin section was placed briefly in an individual water bath, placed on a microscope slide, and dripped with 70% alcohol before being covered with a thin plastic film. The slides were then stacked together, put under pressure using a parallel clamp, and subsequently refrigerated for 14 days at

4°C, to ensure fixation onto the microscope glass. The complete cutting procedure with images of each step is outlined in Appendix A.

Following the 14 days under pressure, the specimens were stained using an osteopontin immunohistochemical (IHC) staining process. This staining procedure targets the osteopontin-rich cement lines separating the BSU, and gives them a bright pink colour, allowing BSU to be distinguished from one another by the now pink cement line surrounding them. After removing the sections from the clamps and peeling off the thin plastic films, the microscope slides were each placed in a vertical capillary receptacle (Figure 3.2), which ensures minimal damage to the sections while providing uniform distribution of the solution that is dripped in the top chamber.

Figure 3.2: Apparatus used to facilitate staining of the microscope slides. The apparatus can hold up to 10 vertical capillary receptacles (only 3 pictured), to allow for easy staining of multiple slides.

The sections were first blocked with 0.5% casein (Sigma-Aldrich; Copenhagen, Denmark) in TBS [0.05 M Tris-HCl (pH 7.6) + 0.15 M NaCl] and an avidin/biotin blocking kit (Dako; Glostrup, Denmark). They were then incubated in a biotinylated goat anti-osteopontin antibody (BAF1433; R&D systems; Minneapolis, MN) diluted in the TBS/casein solution. These antibodies attach to

the osteopontin that is present in high proportions in the cement lines. To increase the intensity of the staining, a secondary rabbit anti-goat antibody (305-065-046; Jackson ImmunoResearch; West Grove, PA) diluted in TBS/casein was applied, and detected with BrightVision poly- alkaline phosphatase-anti-rabbit IgG (VWRKDPVO110AP; ImmunoLogic; Duiven, Netherlands). This step increases the length of the antibody chain, making staining more pronounced when the Liquid Permanent Red (DAKO; Glostrup, Denmark) was applied for visualization. Finally, the sections were mounted to a microscope glass with Aquatex. This staining technique also allows the individual lamellar structures to be seen when placed under a polarized light microscope, further improving the ability to differentiate between BSU (Figure 3.3). The complete staining procedure is described in detail in Appendix B.

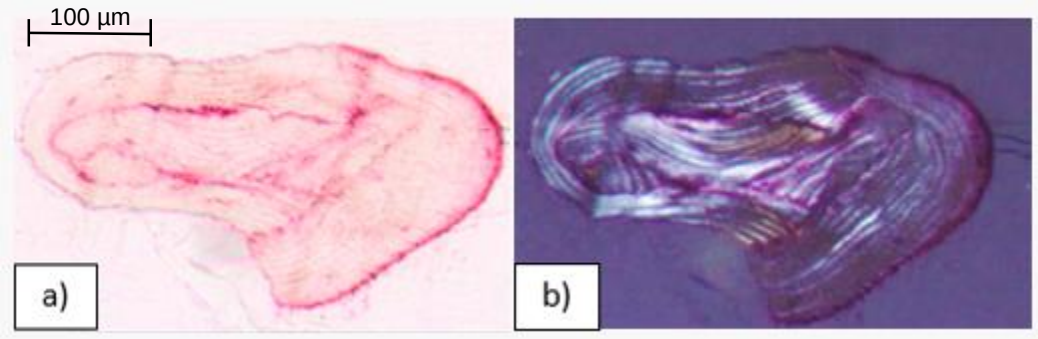

Figure 3.3: A trabecular profile after IHC staining viewed from: a) a high-resolution scan, and b) under a polarized light microscope.

3.3 Data Collection

In order to take quantitative measurements on the prepared slides, they were digitized using a Hamamatsu NanoZoomer 2.0HT high-resolution scanner at x20 magnification and a resolution of 0.46 µm/pixel [92]. From these scans, a 75 mm^2 area of trabecular bone, oriented along the superior-inferior direction of the vertebra, was used for analysis (Figure 3.4).

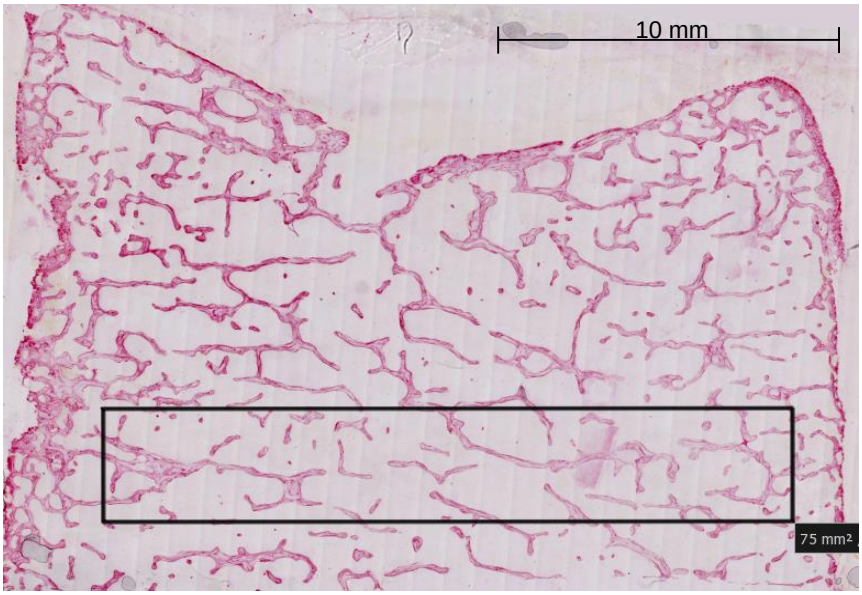

Figure 3.4: A 75 mm² region of a vertebral body used for analysis.

The area of interest was then exported to ImageJ (also known as Fiji), an open source software in which the quantitative analysis was completed [93]. Each trabecular profile was given an identification number for analysis. A profile, for the purpose of this study, is defined as a discrete and continuous area of trabecular bone in the 2-D section; it does not necessarily correspond to a single trabecula in the 3-D structure. This numbering system helped to map out the profiles, allowing for a specific trabecular profile to be easily found. An example of a 25 mm^2 area (1/3rd of the total area analyzed) with trabecular profiles identified may be seen in Figure 3.5.

Figure 3.5: Identification of trabecular profiles in a portion of the analysed area.

Measurements were taken by first calibrating the length scales between the NanoZoomer Digital Pathology viewer [94] and ImageJ. Then, the perimeter around each BSU was drawn by hand. The BSU that were straddling the upper and left boundaries of the 75 mm^2 analysis regions were included in the analysis, while those straddling the lower and right boundaries were not (Figure 3.6). The traced BSU selections of each trabecular profile were saved in ImageJ as regions of interest (ROI), which is essentially a list of points which defines the BSU perimeter as a polygonal shape. This compact mathematical description allows for the retrieval of the selection overlay in the future and the possibility to retake measurements without having to retrace each BSU [95]. Seven morphometric parameters, as summarized in Table 3-2, were measured from each BSU.

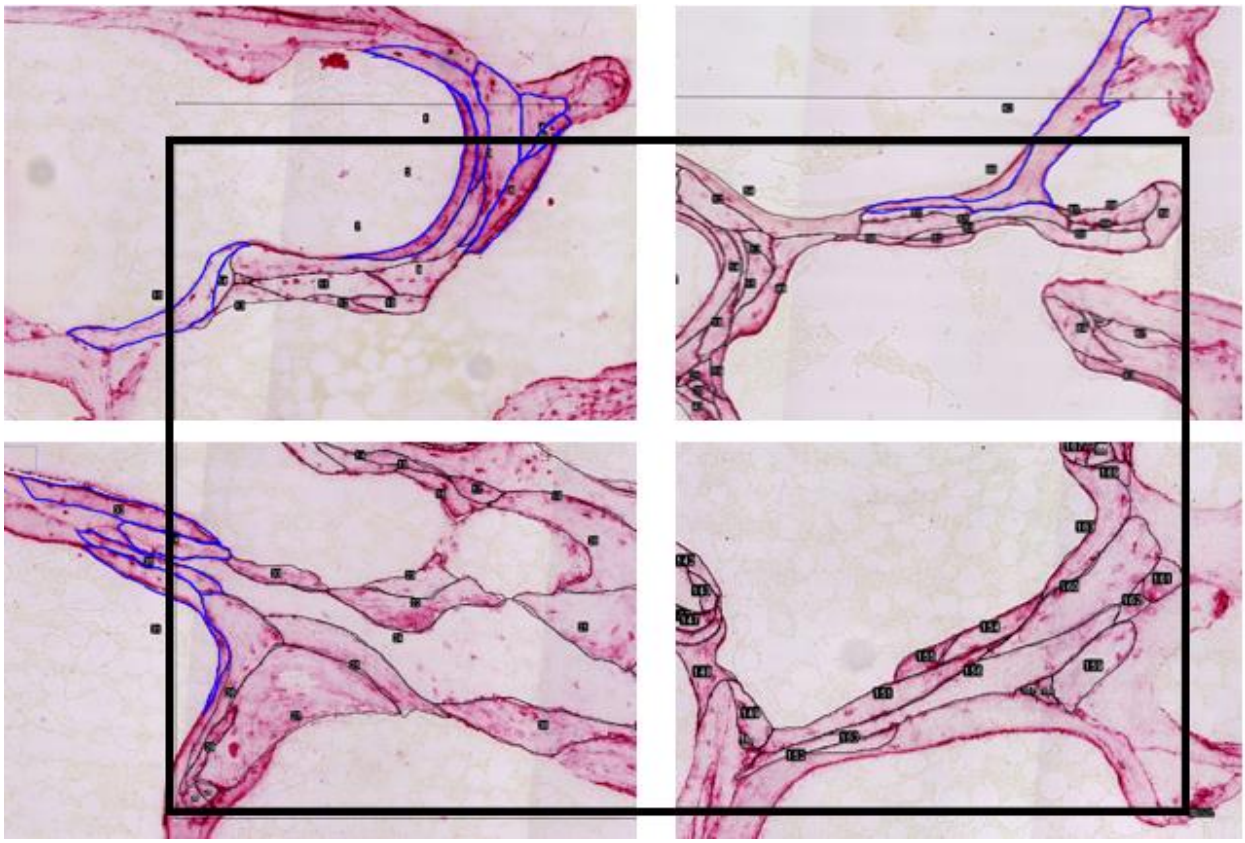

Figure 3.6: The four corners of the 75mm^2 region of analysis illustrating which BSUs were considered for analysis. The BSUs outlined in blue are considered in analysis since they are straddling the upper or left boundary. The BSU crossing the right or lower boundary were not considered.

Table 3-2: Description of BSU parameters measured

BSU Parameter	Unit	Description	Illustration
Area (BSU.A)	μm^2	The area inside of the manually traced selection.	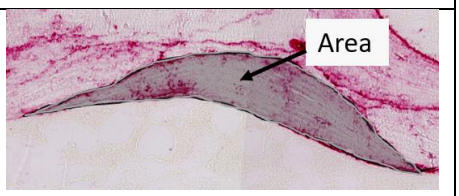
Perimeter (BSU.P)	µm	The length of the tracing.	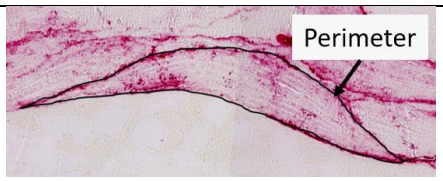
Length (BSU.L)	µm	The direct length (caliper length) between the two farthest points of the selection.	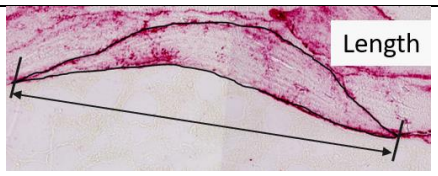
Thickness (BSU.Th)	µm	The diameter of the maximum inscribed circle within the selection. Measurement obtained using plugin [96].	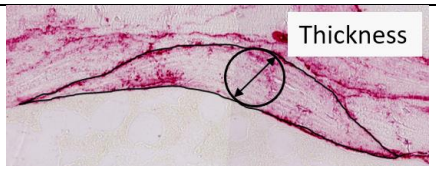
Aspect Ratio (BSU.A.R.)	N/A	A shape descriptor calculated as the ratio of BSU thickness to BSU length.	N/A
Circularity (BSU.Cir)	N/A	A shape descriptor indicative of how compact the selection is. A number between 0 and 1, 1 being a perfect circle, calculated as $(4\pi * \frac{Area}{Perimeter^2})$.	N/A
Solidity (BSU.Sol)	N/A	A shape descriptor indicative of how convex the selection is. A number between 0 and 1, 1 being a perfectly convex shape, calculated as $\frac{Selection\ Area}{Convex\ Area}$.	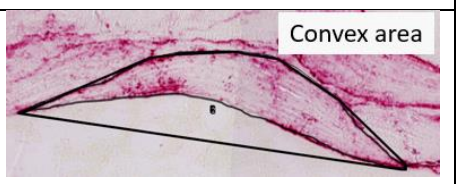

The remodeling age of each BSU was also characterized; BSU were given a designation of 1, 2 or 3 based on the extent to which their shape was altered by subsequent remodeling events. The newest surface BSU, which did not demonstrate any resorption or disruption by more

recent remodeling, were given a 1. Surface BSU that had been slightly remodeled over but where their thickness was still intact were given a 2. Interior BSU that were completely surrounded by other BSU were given a 3 (Figure 3.7). These categories would allow us to compare, for example, differences in the parameters of interest between old and young for only the newest BSU. Doing so allows the complex effects of remodeling to be ignored.

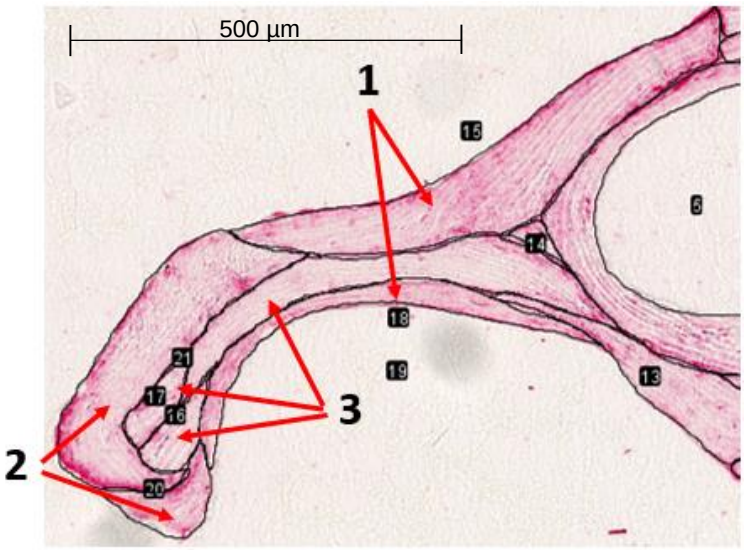

Figure 3.7: *Example of numbers given to BSUs based on the extent which they've been remodeled over.*

Furthermore, each trabecular profile area (TP.A) and perimeter (TP.P) were recorded. These values were used to calculate two derived parameters: the number of BSU per trabecular profile area (#BSU/TP.A), and the cement line length in a given trabecular profile (CL.L/TP.A). The cement line length (CL.L) was defined as:

$$CL.L = \frac{1}{2}[(\sum BSU.P) - (TP.P)] \quad (1)$$

which has units of mm. When normalized by the area of the trabecular profile (TP.A), it becomes:

$$\frac{CL.L}{TP.A} = \frac{(\sum BSU.P) - (TP.P)}{2(TP.A)} \quad (2)$$

with units of mm/mm^2.

3.4 Data Analysis

Measurements were recorded in an Excel spreadsheet, and organized by specimen number, trabecular profile number, and finally BSU number. In a separate spreadsheet, the BSU parameters were averaged for each profile, which enabled the cement line per profile area (CL.L/TP.A) and the number of BSU per profile area (#BSU.TP.A) to be calculated. The specimen averages were tabulated for each of the parameters of interest in a third sheet.

Statistical analysis of the results was performed in either Stata or GraphPad Prism. Three separate sets of analyses were conducted and are described in the following subsections. The first was a repeatability analysis. Multiple measures of the BSU in one trabecular profile were performed to provide some indication of the repeatability of the user-performed tracing. Next, only the BSU that did not demonstrate any subsequent resorption or bone formation (i.e. the ones given a designation of 1) were analyzed. This subset was chosen to allow comparison with earlier results [26,28–31] and because the geometries of these BSU have yet to be altered by remodeling which makes them the most representative of the BSU being created at that time in the patient's skeletal history. Since this subset of BSU represents the "newest" remodeling events, they will henceforth be referred to as BSU_{new}, to easily distinguish them from those used in the final set of analyses which includes all BSU within the region of analysis. A value of $p<0.05$ was considered significant for all analyses, and is presented in bold on the graphs.

3.4.1 Repeatability Analysis

In order to determine the repeatability of our measurements, 20 BSU of a trabecular profile (Figure 3.8) were measured an additional 10 times. The 10 additional measurements were taken over a five-day period, to avoid fatigue, any memory effects, and to best simulate a "fresh" tracing attempt. For each BSU within the profile, BSU.A, BSU.Th, and BSU.L were measured, along with the CL.L/TP.A. These 10 repeated measurements, along with the original measurements, were used to determine the standard error (standard deviation), and the relative standard error

(calculated as standard deviation divided by the mean) associated with manually drawing around each BSU.

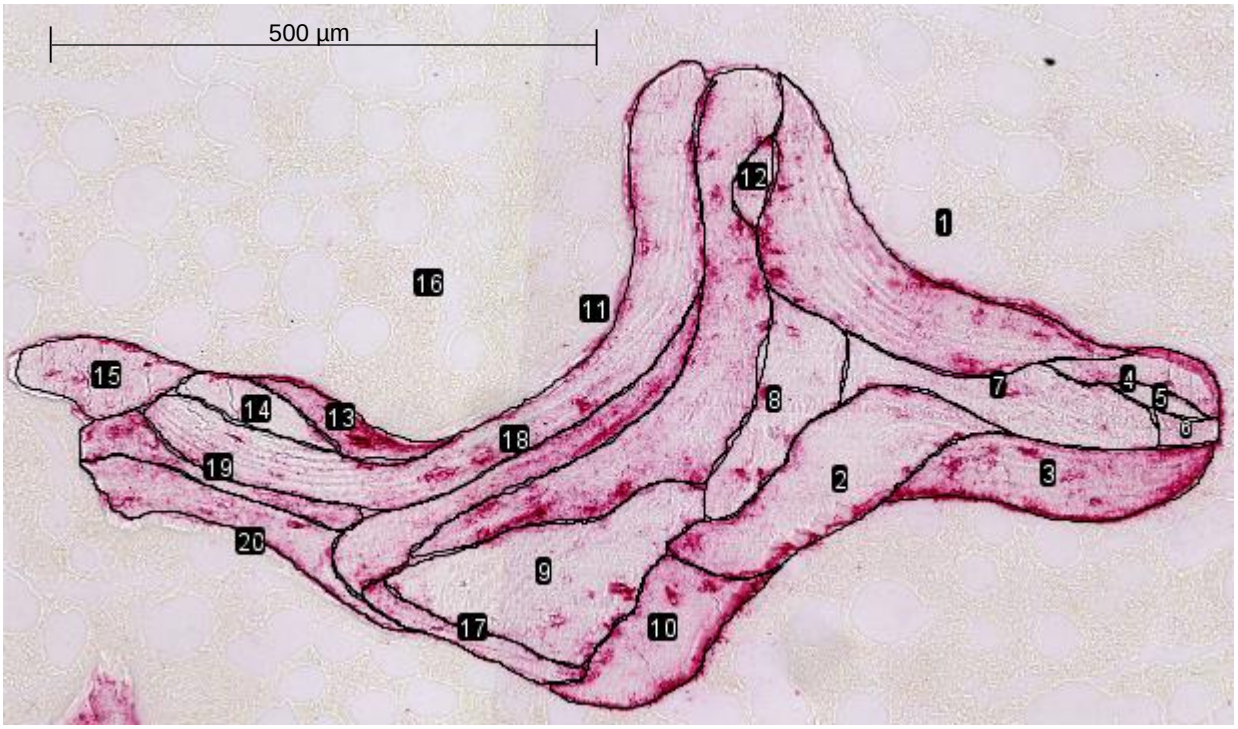

Figure 3.8: Trabecular profile with 20 BSU that were measured on 10 additional occasions to determine the repeatability of manual measurements.

3.4.2 Analysis of intact BSU (BSU_{new})

For the analyses using only the intact surface BSU, Stata was first used to determine whether the BSU_{new} morphological parameters were significantly different between the two age groups (StataCorp LLC; College Station, TX). This was done by finding the best fit models for the frequency distributions from three mixed-effect models, namely, a normal (Gaussian), negative-binomial, or gamma distribution. When the frequency distributions were plotted for visualization, they demonstrated positive- or right-skewed distributions, which negative-binomial and gamma models are often used to fit. The best fit model was identified on logical grounds, as there were not enough specimens in this study to justify a statistical comparison between models. However, if two models fit the data similarly, analysis was performed for both models to ensure the conclusions would not depend on the model selected.

Mixed-effect models are equipped to handle nested data. The BSU data collected in this study are considered to be nested because there are varying numbers of data points in each individual, and each individual is part of an age group, meaning each data point is not independent. In these analyses, the data points were grouped by the specimen in which they were taken. Analyzing each measurement as independent would artificially inflate the results. Because of the nested nature, the generally right- or positive-skewed distributions, and the small number of individuals analyzed, no other distributions were considered due to a risk of overstating the results or breaching assumptions. The mean was used to quantify the between-group differences if the data followed a normal distribution, while the median was used to quantify negative-binomial or gamma distributions, which is best practice when the distribution is skewed. The distribution plots are included herein simply to illustrate the skewed distribution and the range of values obtained for the morphometric measures for each age group; they had no bearing in the statistical analysis, and the curves within them are not necessarily representative of the mixed-effect model selected.

The values for BSU_{new}.A, BSU_{new}.Th, BSU_{new}.L, BSU_{new}.A.R, BSU_{new}.Cir, and BSU_{new}.Sol for each intact BSU (2,391 young and 1,839 old) were analyzed in Stata. The regression results of the best-fit models were used to quantify differences between the two age groups. The differences, if significant, were quantified by a z-value, which is a standardized variable given when using a mixed-effect model (similar to a t-score). It is evaluated with reference to a standard normal distribution and reflects the strength of the group effect within the regression. The combination of a z-value, the p-value, and the mean/median would allow the model to be reconstructed, without the need for complex regression equation variables.

In addition to simply detecting differences between the young and old groups, linear regression was also used to detect significant relationships between the BSU morphological parameters and various independent variables (e.g., age and the 3-D architectural parameters).

Each individual's median values for BSU_{new}.A, BSU_{new}.Th, and BSU_{new}.L were analyzed in GraphPad Prism. Additionally, BSU_{new}.Th was normalized by Tb.Th in order to determine if any changes in BSU_{new}.Th could be accounted for by a change in Tb.Th. For all these parameters, linear regression was performed with respect to age, and with respect to the individual's 3-D architectural parameters measured in the vertebra (BV/TV, SMI, Conn. D., Th. N, Tb.Th, Tb.Sp). The results are presented as the p-values indicating if the slopes are significantly non-zero, as well as the slope equations, defined as:

$$y = slope(x) + intercept \quad (3)$$

where y is the BSU_{new} parameter, and x is the age or 3-D architectural parameter.

3.4.3 Analysis of all BSU

For the second analysis, the values for BSU.A, BSU.Th, BSU.P, BSU.L, BSU.A.R, BSU.Cir, and BSU.Sol of all BSU within the region of analysis (9,901 young, 6,950 old) were analyzed in Stata, along with the two derived parameters of #BSU/TP.A and CL.L/TP.A. Although it was not included in the BSU_{new} analyses, BSU.P was included when considering all BSU because it is used to calculate CL.L/TP.A. Again, the best fit models were determined, and the regression results of the selected models were reported. Values for the medians/means, the z-values, and the p-values were used to quantify significant differences between the distributions of the two groups. The distribution plots are also included herein for illustrative purposes, but had no bearing in the statistical analysis of the frequency distributions.

Linear regression was then performed for the specimen medians of BSU.A, BSU.Th, BSU.Th/Tb.Th, BSU.P, BSU.L, #BSU/TP.A, and the mean of CL.L/TP.A with respect to the individual's age and their 3-D architectural parameters. The results are presented as p-values, indicating if the slope is significantly non-zero, accompanied by the slope equations and r^2 values.

4 Results

A total of 16,853 BSU were measured between the 16 individuals, 4,230 of which were considered BSU_{new} and used in the first study. The smaller subset of unaltered BSU_{new} was first studied to provide a baseline of age-induced morphometric changes. It also allowed for easier comparisons with previously published data. All BSU were then analysed. The results of these two analyses are outlined in Section 4.2 and 4.3. The repeatability study is presented first, however, to establish the experimental error associated with the manual tracing of BSU.

4.1 Repeatability analysis

A total of 11 measures —the original plus ten repeats— were made on the 20 BSU shown in Figure 3.8. The standard error was found to increase with BSU.A, but was independent of BSU.Th and BSU.L (Figure 4.1). These values are reasonable because of the way that BSU.Th and BSU.L are measured. It can be difficult to focus in on large BSU as it is restricted to the size of the computer monitor, so error in the area is expected to increases with the size of BSU. However, BSU.L and BSU.Th are measured essentially as the primary (long) and secondary (short) axes of the selection, and small inaccuracies in manual drawing would not be expected to significantly impact these parameters.

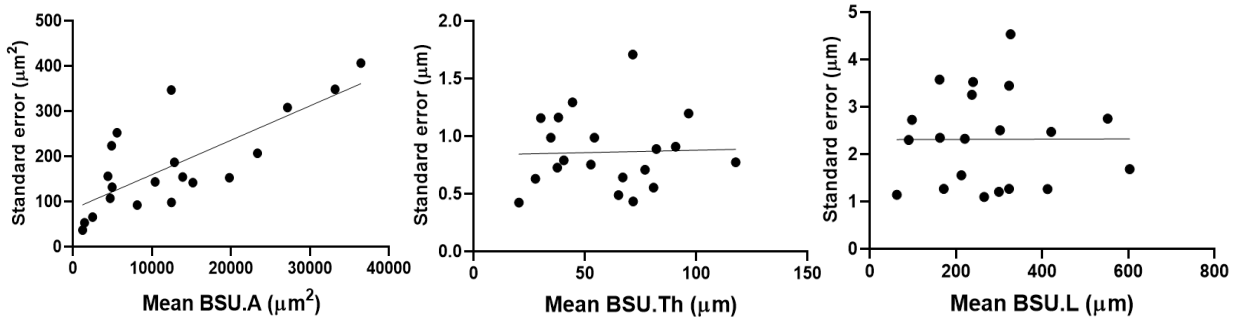

Figure 4.1: Standard error of the 11 repeated measures of BSU.A, BSU.Th, and BSU.L of the 20 BSU in the trabecular profile of Figure 3.8.

The relative standard error is also reported, and it was found to be <5% of the mean of the 11 measurements for BSU.A, BSU.Th and BSU.L (Figure 4.2). It may be observed that the relative error decreases as BSU.A, BSU.Th, and BSU.L increases. This trend is logical because

small deviations from the true BSU perimeter during manual tracing are expected regardless of the size of the BSU measured, and normalizing the error by a larger BSU would decrease the relative error.

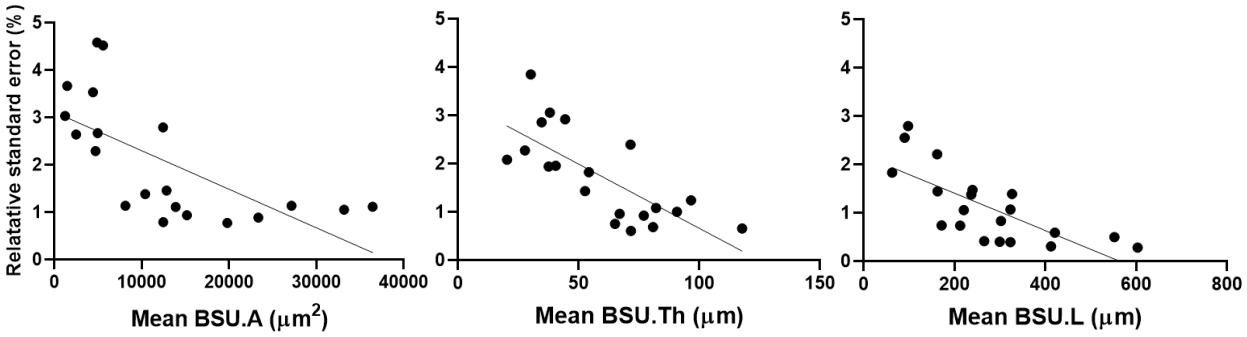

Figure 4.2: Relative standard error of the 11 repeated measures of BSU.A, BSU.Th, and BSU.L of the 20 BSU in the trabecular profile of Figure 3.8.

Further, the relative standard error for CL.L/TP.A was 0.44%, making it the most repeatable parameter to measure. As will be shown in the subsequent sections, the decreases in the medians of parameters that had significant changes between the young and old groups were all >15%. These results are still robust even in the worst-case scenario of a 5% error. Additionally, because the errors are random for BSU.Th and BSU.L, they would cancel each other out for these parameters.

4.2 Results of intact BSU (BSU_{new})

The summary statistics of the individual's age and their median values for $BSU.A_{new}$, $BSU.Th_{new}$, BSU_{new}.Th/Tb.Th, and BSU_{new}.L are presented in Table 4-1. The 95% confidence intervals for the medians have also been included in brackets. It must be noted, however, that confidence intervals for medians may not be very robust.

Table 4-1: Subject age, number of unaltered BSU measured (n), and their median BSU_{new}.A, BSU_{new}.Th, BSU_{new}.Th/Tb.Th and BSU_{new}.L [95% CI].

	Age	*n*	BSU_{new}.A (μm^2)	BSU_{new}. Th (μm)	BSU_{new}.Th /Tb.Th (μm/μm)	BSU_{new}.L (μm)
Young	**18.5**	202	7770 [6497-9647]	45.1 [40.5-52.0]	0.334 [0.300-0.385]	248 [228-282]
	21.4	278	8528 [7474-9941]	45.1 [41.2-49.4]	0.344 [0315-0.377	291 [270-310]
	21.7	300	9873 [7884-11567]	51.0 [45.7-54.3]	0.381 [0.341-0.406]	268 [246-305]
	26.2	305	5293 [4067-6344]	34.0 [31.3-38.1]	0.318 [0.292-356]	194 [178-230]
	30.2	340	7166 [6407-7949]	47.2 [45.2-52.2]	0.387 [0.371-0.428]	204 [186-225]
	35.7	319	6894 [6163-7943]	42.1 [39.8-43.8]	0.354 [0.334-0.368]	243 [218-260]
	36.2	385	5777 [5115-6452]	41.9 [40.5-44.1]	0.355 [0.343-0.374]	182 [168-199]
	37.6	262	10929 [9224-12592]	57.3 [53.5-62.2]	0.400 [0.374-0.435]	258 [224-292]
Old	**69.1**	232	3698 [3103-4107]	32.1 [28.6-34.6]	0.300 [0.267-0.324]	153 [138-170]
	71.6	195	7145 [5690-8338]	49.2 [44.9-54.6]	0.279 [0.255-0.310]	210 [187-238]
	73.5	181	4071 [3431-5152]	33.5 [29.0-36.2]	0.187 [0.162-0.202]	167 [134-202]
	77.3	189	6774 [5570-8046]	39.4 [36.0-43.0]	0.342 [0.314-0.374]	228 [197-258]
	78.0	260	3839 [3220-4447]	33.6 [31.8-36.4]	0.273 [0.258-0.296]	161 [149-180]
	83.0	233	3678 [3408-4730]	33.9 [31.2-36.7]	0.308 [0.284-0.334]	157 [145-173]
	85.8	321	3222 [2859-3656]	29.2 [27.6-30.9]	0.281 [0.266-0.297]	161 [150-178]
	96.4	228	6522 [5648-7463]	44.7 [40.6-47.8]	0.300 [0.273-0.319]	210 [188-233]

The analysis in Stata revealed significant differences in BSU_{new}.A, BSU_{new}.Th, and BSU_{new}.L between the young and old groups (Figure 4.3). All parameters followed a mixed-effect gamma model, which also accounted for the nested nature of the data and the different number of measurements for each sample. Specifically, BSU_{new}.A was significantly lower (z=2.91, p=0.004) in the old group (median = 4442 μm^2) compared to the young group (median= 6797 μm^2). There was a significant reduction in BSU_{new}.Th (z=2.81, p=0.005) in the old (median = 35.1

μm) compared to the young (median = 44.0 μm). BSU_{new}.L was also significantly smaller (z=3.07, p=0.002) with age (old: median= 177.3 μm; young: median = 230.0 μm).

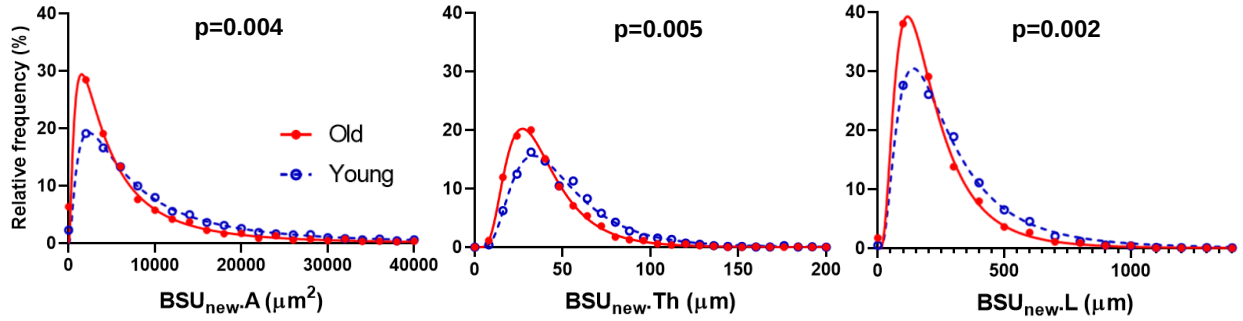

Figure 4.3: Frequency distribution plots for the area, thickness and length of the surface BSU that are not affected by subsequent remodeling. The curves shown are polynomials fit to the data.

The between-group differences were then analyzed for the three shape descriptors. All three shape descriptors followed mixed-effect gamma models, though no significant differences were found between the two groups for BSU_{new}.A.R. (p=0.86), BSU_{new}.Cir (p=0.90), or BSU_{new}.Sol (p=0.52), (Figure 4.4).

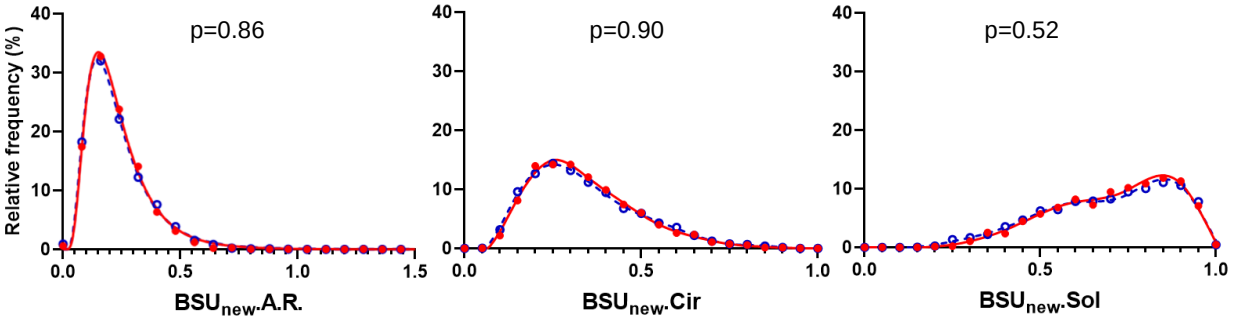

Figure 4.4: Distribution plots for the aspect ratio, circularity and solidity of the surface BSU that are not affected by subsequent remodeling. The curves shown are polynomials fit to the data.

Linear regression in GraphPad Prism revealed that BSU_{new} morphometry is related to both age and to two of the 3-D architectural parameters investigated (BV/TV and SMI), as shown in Figure 4.5. Significant negative linear correlations were found between the age of the individuals and their median BSU_{new}.A (p=0.0096), BSU_{new}.Th (p=0.0496), and BSU_{new}.L (p=0.0066). Negative correlations were also observed with SMI for BSU_{new}.A (p=0.0011), BSU_{new}.Th (p=0.0043), and BSU_{new}.L (p=0.0018). Conversely, significant positive linear correlations between

bone volume fraction (BV/TV) and median BSU_{new}.A (p=0.0003), BSU_{new}.Th (p=0.0030) and BSU_{new}.L (p=0.0007) were found. When BSU_{new}.Th was normalized by Tb.Th, the changes were still significant with age (p=0.0077), BV/TV (p=0.0019), and SMI (p=0.0009). No correlation was observed between the 2-D parameters and Conn. D (p>0.7050), Tb.N (p>0.0685), Tb.Sp (p>0.0987), or Tb.Th (p>0.0956).

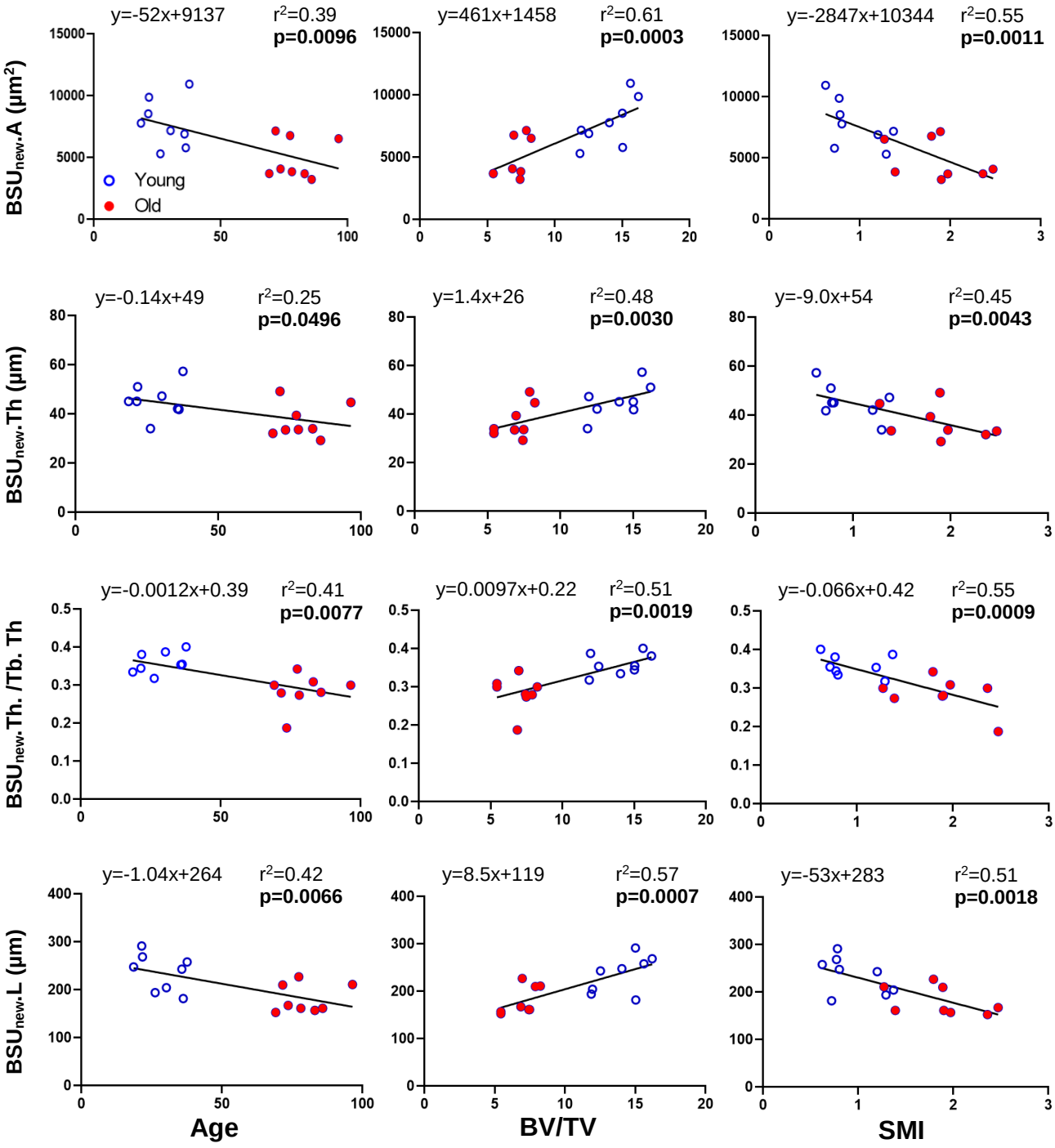

Figure 4.5: Linear regressions for $BSU_{new}.A$, $BSU_{new}.Th$, $BSU_{new}.Th/Tb.Th$, and $BSU_{new}.L$ with respect to age, BV/TV and SMI.

4.3 Results of all BSU

The summary statistics of the morphometric parameters measured on all the BSU are presented in Table 4-2, while the derived profile parameters (#BSU/TP.A and CL.L/TP.A) are presented in

Table 4-3. All values are presented as medians because the data followed right-skewed distributions, except for the CL.L/TP.A which followed a Gaussian model and is represented with a mean. Again, the 95% confidence intervals of the medians (mean for CL.L/TP.A) have been included in brackets.

Table 4-2: Subject age, number of all BSU measured (n), and their median BSU.A, BSU.Th, BSU.Th/Tb.Th, BSU.P, and BSU.L.

	Age	*n*	BSU. A (μm^2)	BSU. Th (μm)	BSU.Th/Tb.Th (μm/μm)	BSU.P (μm)	BSU. L (μm)
Young	**18.5**	791	5682 [5377-6208]	44.7 [42.4-46.5]	0.331 [0.314-0.344]	428.6 [405.1-463.0]	187.4 [175.3-201.1]
	21.4	1298	5793 [5428-6404]	44.3 [42.9-45.8]	0.338 [0.328-0.349]	458.2 [437.8-485.4]	201.9 [191.8-210.9]
	21.7	1341	5985 [5582-6434]	45.8 [44.4-48.1]	0.342 [0.332-0.359]	421.3 [408.3-439.8]	181.0 [170.5-190.8]
	26.2	1491	3572 [3315-3853]	32.7 [31.8-34.0]	0.305 [0.297-0.318]	361.4 [342.9-377.3]	151.2 [146.3-162.9]
	30.2	1186	5270 [4893-5795]	44.1 [42.9-45.7]	0.361 [0.352-0.374]	394.5 [375.7-410.4]	163.8 [156.3-171.9]
	35.7	1526	4284 [4062-4493]	37.2 [36.2-38.0]	0.312 [0.304-0.320]	380.1 [367.9-397.5]	165.2 [158.3-171.0]
	36.2	1348	4492 [4076-4720]	41.6 [40.7-42.8]	0.352 [0.345-0.362]	361.1 [346.1-376.7]	151.1 [146.2-158.0]
	37.6	920	6990 [6431-7510]	50.0 [48.1-51.4]	0.350 [0.336-0.360]	444.4 [423.5-466.3]	191.0 [179.4-202.6]
Old	**69.1**	1004	2128 [1960-2301]	28.2 [27.0-29.1]	0.263 [0.252-0.272]	258.6 [243.7-272.6]	102.8 [98.4-108.5]
	71.6	749	5570 [5159-5962]	47.6 [45.1-49.4]	0.270 [0.256-0.281]	390.2 [367.5-419.8]	169.0 [155.0-178.6]
	73.5	664	3733 [3214-4176]	35.5 [33.1-37.6]	0.198 [0.185-0.210]	350.8 [323.2-364.9]	143.5 [133.7-157.8]
	77.3	847	4202 [3897-4739]	38.3 [36.6-40.1]	0.333 [0.319-0.347]	372.0 [351.8-398.1]	157.7 [148.6-167.6]
	78.0	894	3751 [3437-4010]	37.2 [35.4-38.7]	0.303 [0.288-0.314]	347.1 [328.1-363.1]	145.8 [138.1-152.9]
	83.0	825	3484 [3252-3687]	35.8 [34.4-36.7]	0.325 [0.313-0.334]	328.6 [311.8-355.7]	136.2 [128.0-147.6]
	85.8	1290	3330 [3135-3493]	32.7 [31.4-33.6]	0.314 [0.302-0.323]	330.7 [318.2-344.6]	147.3 [138.8-153.0]
	96.4	677	5751 [5393-6248]	45.2 [44.0-47.8]	0.304 [0.295-0.321]	410.8 [401.2-431.7]	175.3 [166.3-187.3]

Table 4-3: Subject age, number of profiles measured (n), and their median TP.A, #BSU/TP.A and mean CL.L/TP.A.

	Age	*n*	TP.A (mm^2)	#BSU/TP.A (BSU/mm^2)	CL.L/TP.A (mm/ mm^2)
Young	**18.5**	53	0.0680 [0.0409-0.1189]	119.1 [103.0-157.1]	21.0 [19.4-22.6]
	21.4	40	0.1310 [0.0787-0.2529]	135.9 [110.1-183.3]	25.6 [23.3-27.9]
	21.7	108	0.0816 [0.0668-0.1518]	134.4 [103.0-171.6]	22.0 [20.2-23.8]
	26.2	85	0.0399 [0.0238-0.0561]	214.3 [170.9-302.3]	33.1 [30.5-35.6]
	30.2	87	0.0341 [0.0250-0.0509]	196.4 [156.9-243.2]	25.0 [23.3-26.7]
	35.7	82	0.0416 [0.0314-0.0802]	215.7 [192.4-261.6]	30.0 [28.6-31.5]
	36.2	82	0.0421 [0.0358-0.0582]	204.7 [167.4-237.1]	26.0 [23.9-28.2]
	37.6	51	0.1094 [0.0715-0.2103]	102.4 [84.9-127.6]	19.1 [17.4-20.8]
Old	**69.1**	105	0.0179 [0.0140-0.0219]	419.0 [359.0-505.0]	39.9 [37.8-42.0]
	71.6	48	0.0671 [0.0288-0.0839]	162.3 [120.5-248.3]	24.6 [21.8-27.3]
	73.5	59	0.0166 [0.0100-0.0295]	430.7 [238.5-552.9]	32.7 [29.3-36.0]
	77.3	52	0.0237 [0.0169-0.0572]	274.7 [168.7-387.2]	30.6 [28.0-33.2]
	78.0	78	0.0239 [0.0172-0.0517]	249.4 [201.9-348.3]	29.8 [27.6-31.9]
	83.0	96	0.0190 [0.0125-0.0278]	307.4 [244.8-336.1]	29.0 [27.1-30.9]
	85.8	58	0.0379 [0.0213-0.0944]	263.8 [232.0-352.9]	32.3 [29.8-34.8]
	96.4	53	0.0573 [0.0313-0.0908]	136.8 [117.0-187.6]	21.4 [19.4-23.4]

Unlike with the analysis of the most recent BSU, only one of the size parameters was found to be different between the old and young when all BSU were included. The analysis in Stata revealed that there was a significant decrease in BSU.L (z= 2.15, p=0.031) between the young (median= 206.2 µm) and old groups (median= 172.8 µm), which was best described by a negative binomial model. Additionally, BSU.P was significantly larger (z=2.28, p=0.23) in the young group (398.7 µm) compared to the old group (342.3 µm), and also followed a negative binomial model. BSU.A (p=0.069) and BSU.Th (p=0.077) were best described using gamma models, but were not significantly different between the young and old groups in this analysis (Figure 4.6).

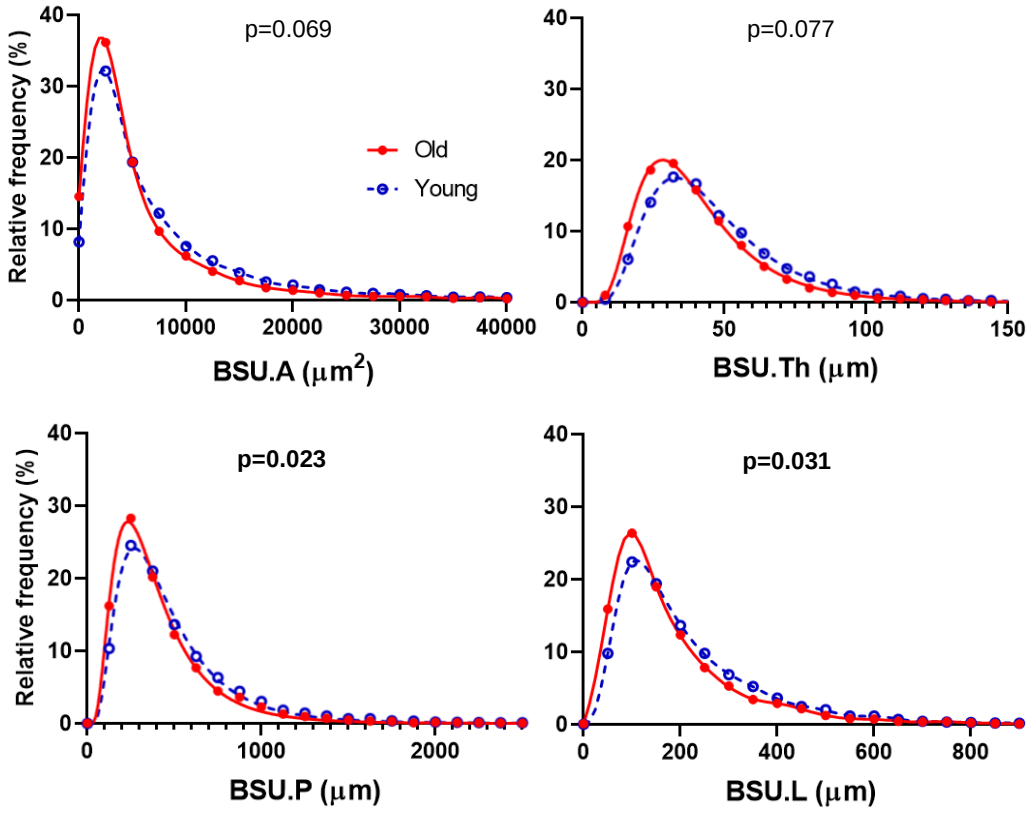

Figure 4.6: Frequency distribution plots for BSU.A, BSU.Th, BSU.P, and BSU.L. The p-value for BSU.L and BSU.P are in bold because they were the only parameters demonstrating significant between-group differences.

The between-group differences were then analyzed for the three shape descriptors. All three were fit with gamma models, but no significant differences were found between the young and old groups for BSU.A.R. (*p*=0.67.), BSU.Cir (*p*=0.63), or BSU.Sol (*p*=0.58), (Figure 4.7).

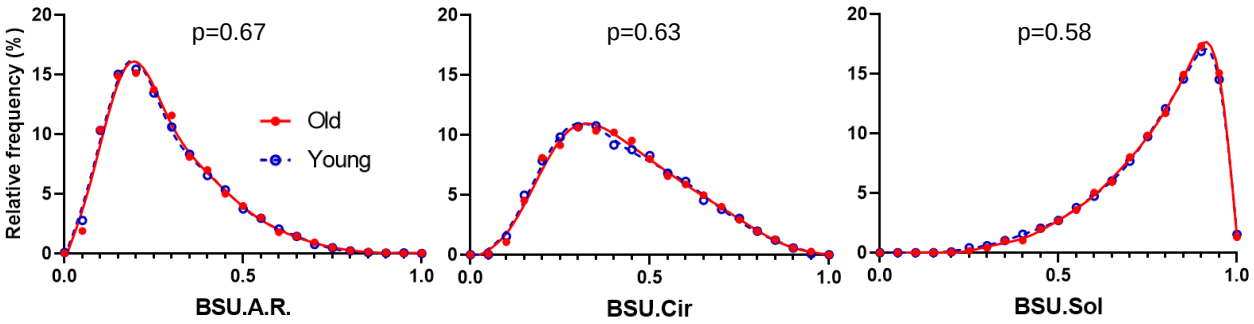

Figure 4.7: Frequency distribution plots for BSU.A.R., BSU.Cir, and BSU.Sol.

The analysis of the profile metrics revealed that #BSU/TP.A was significantly different between the young and old groups (z=3.12, p=0.002) and followed a gamma model; the old group was found to have more BSU per unit area (median=292 BSU/mm^2) compared to the young (median=172 BSU/mm^2). Unlike any of the other parameters, the CL.L/TP.A frequency distribution followed a normal (Gaussian) curve. The old group had significantly more cement line per unit area (mean=31.0 mm/mm^2) compared to the young group (mean=26.0 mm/mm^2), (z=2.02, p=0.043), (Figure 4.8).

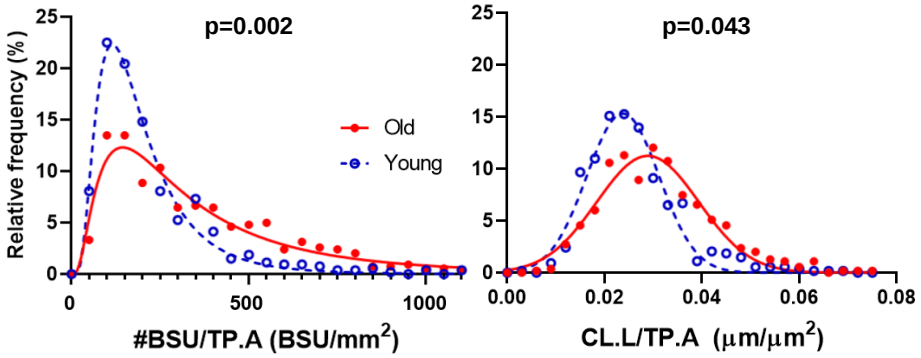

Figure 4.8: Frequency distribution plots for #BSU/TP.A and CL.L/TP.A.

Linear regression revealed that the median BSU.P (p=0.0323) and BSU.L (p=0.0427) were the only BSU parameters which demonstrated a significant linear correlation with age. No correlation was found between the individual's age and their median BSU.A (p=0.0898) or BSU.Th (p=0.1811). When these BSU parameters were plotted as a function of the individual's BV/TV, there was a positive linear correlation between BV/TV and median BSU.A (p=0.0030), BSU.Th (p=0.0127), BSU.P (p=0.0012), and BSU.L (p=0.0016). Linear regression was then performed on

the 2-D parameters with respect to the individual's SMI. A negative linear correlation was found between SMI and median BSU.A (p=0.0015), BSU.Th (p=0.0056), BSU.P (p=0.0006), and BSU.L (p=0.0057) (Figure 4.9).

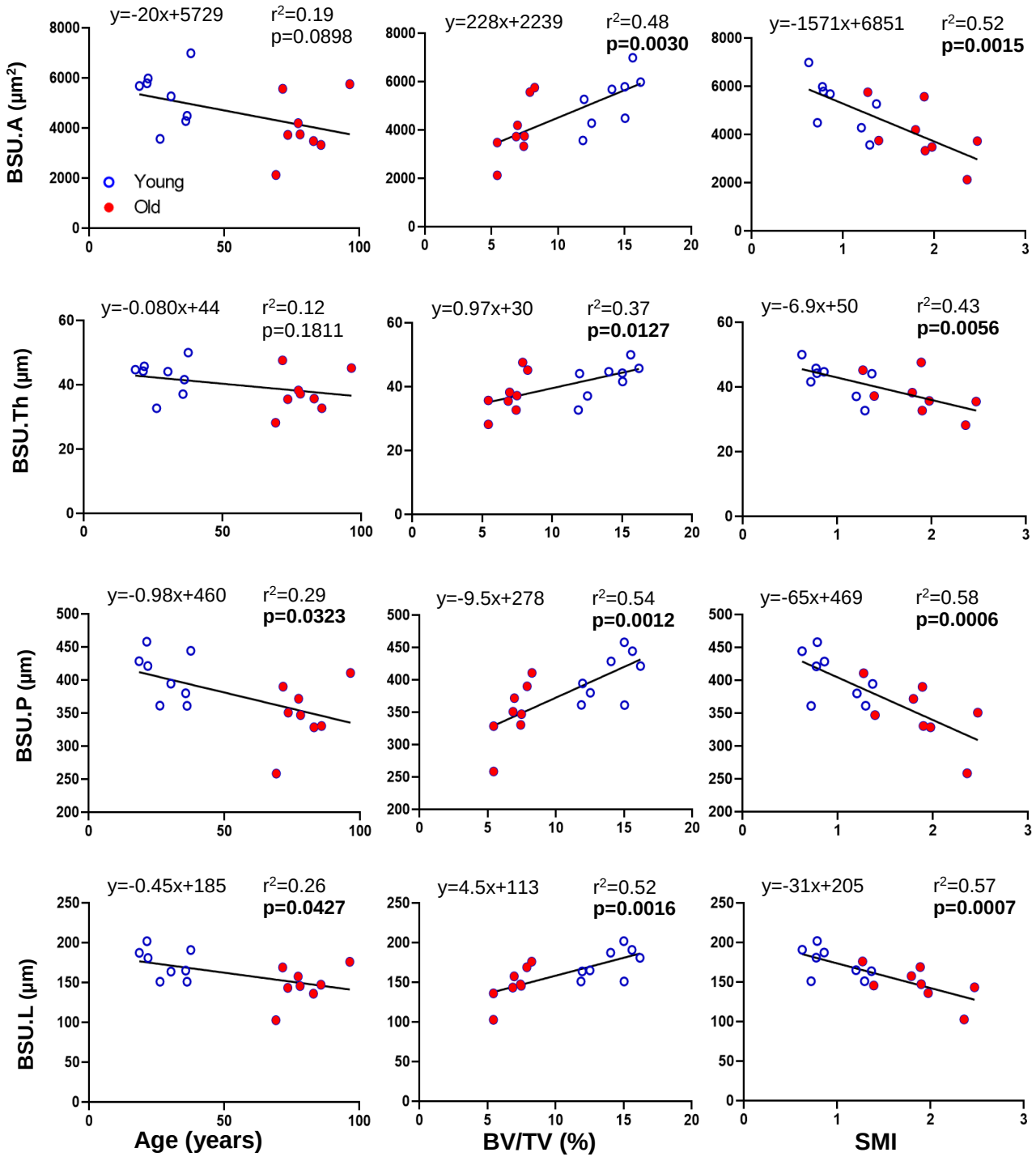

Figure 4.9: Linear regressions of BSU.A, BSU.Th, BSU.P and BSU.L as a function of age, BV/TV, and SMI. The bold p-values indicate that the linear regression slope is significantly non-zero (p<0.05).

Additionally, Tb.Th was found to be positively correlated with BSU.Th (p=0.0313), but not with BSU.A (p=0.0549), BSU.P (p=0.1237), or BSU.L (p=0.1622) (Figure 4.10).

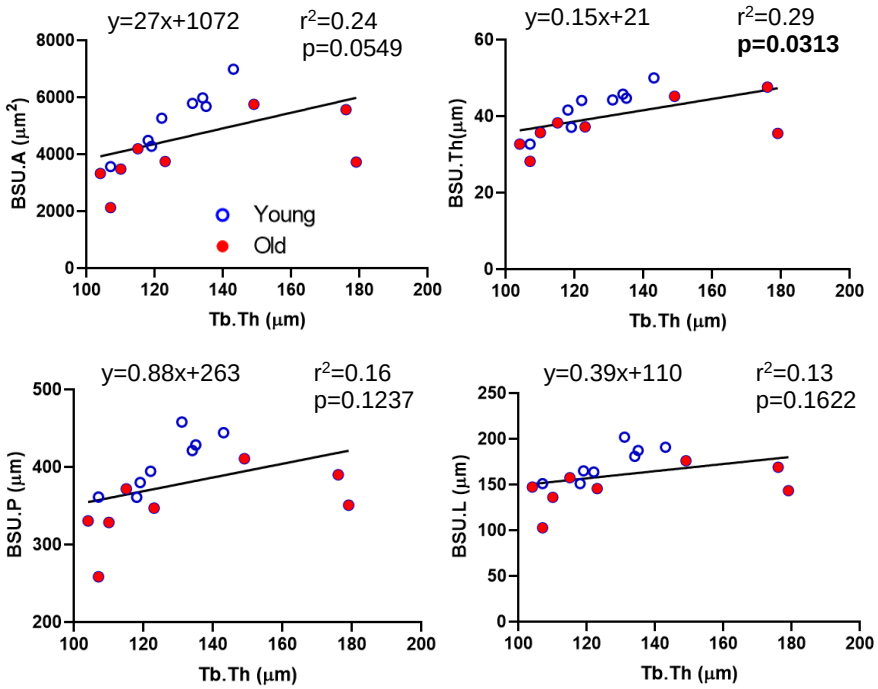

Figure 4.10: Linear regression of BSU.A, BSU.Th, BSU.P, and BSU.L as a function of Tb.Th. The bold p-values indicate that the linear regression slope is significantly non-zero (p<0.05).

Again, BSU.Th was normalized by the 3-D Tb.Th to determine if changes in BSU.Th with respect to age, BV/TV, and SMI can be accounted for by changes in Tb.Th. Significant correlations were found between BSU.Th/Tb.Th and BV/TV (p=0.0122) and SMI (p=0.0008), but still not with age (p=0.0588) (Figure 4.11). No significant linear correlations were found with any of the 3-D morphometric parameters and Conn.D (p>0.53), Tb.N (p>0.22), or Tb. Sp (>0.35).

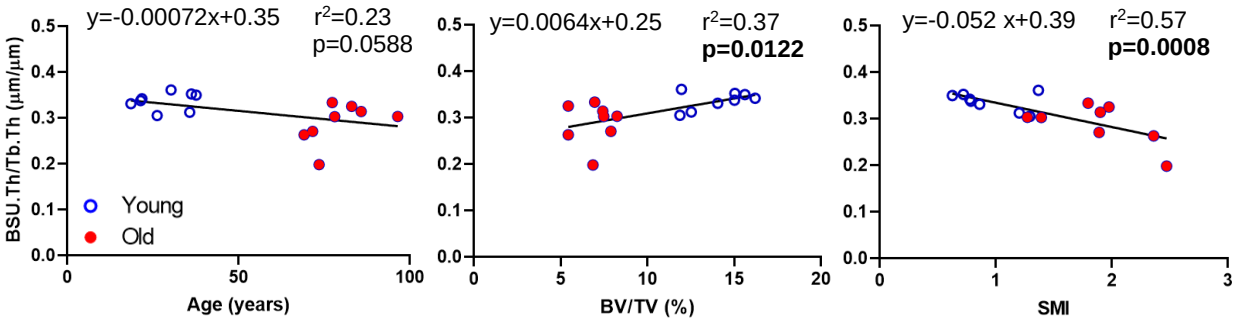

Figure 4.11: Linear regression of BSU.Th/Tb.Th with respect to age, BV/TV and SMI.

When analysing the derived parameters, a negative linear correlation with age was found for the median #BSU/TP.A (p=0.0461), but not with mean CL.L/TP.A (p=0.1827). When these parameters were plotted against BV/TV, both #BSU/TP.A (p=0.0012) and CL.L/TP.A (p=0.0084) demonstrated a significant negative correlation. SMI was very highly correlated to #BSU/TP.A (p<0.0001), and was also correlated to CL.L/TP.A (p=0.0012). These linear regression graphs may be observed in Figure 4.12. No correlations were found between the two derived parameters and Conn.D (p>0.32), Tb.N (p>0.16), Tb.Th (p>0.11), or Tb.Sp (p>0.28).

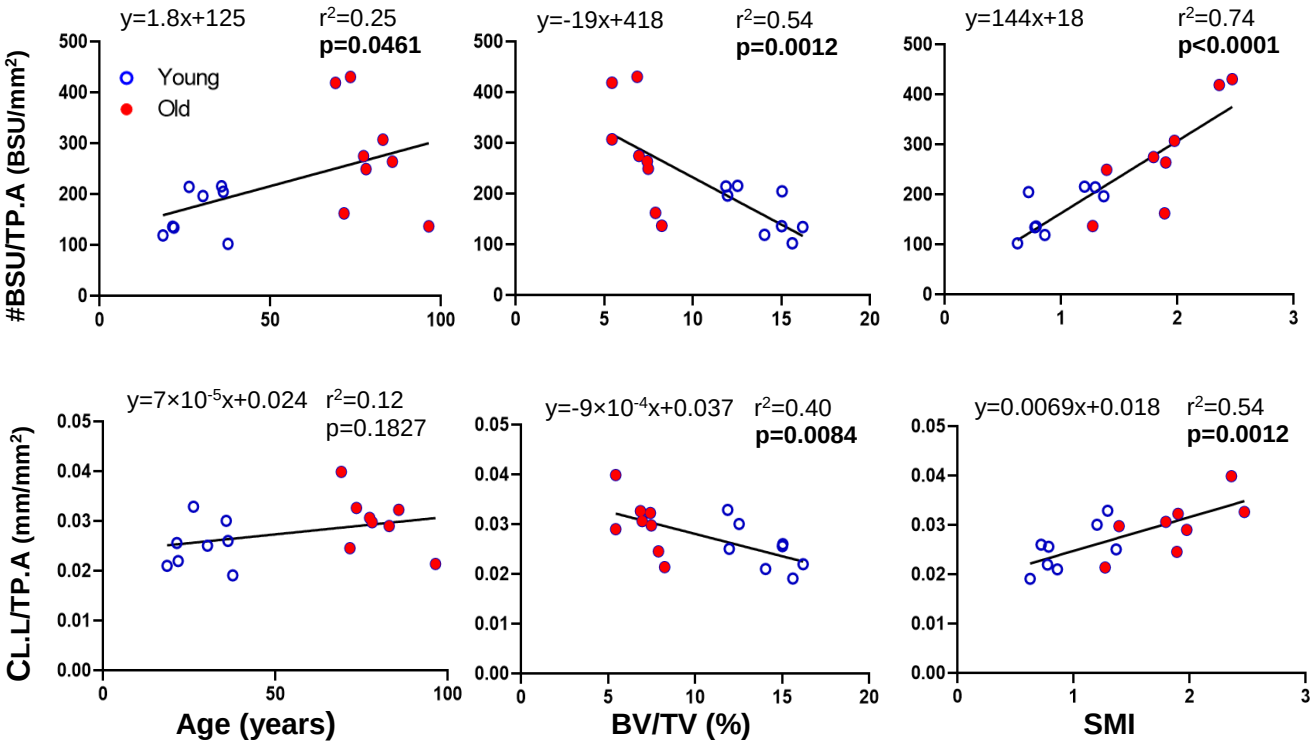

Figure 4.12: Linear regressions of #BSU/TP.A and CL.L/TP.A with respect to age, BV/TV and SMI. The bolded p-values indicate that the slope is significantly non-zero (p<0.05).

5 Discussion & conclusions

5.1 Introduction

The assessment of fracture risk in the elderly is crucial to avoid costly hospital visits and long recovery times. Early identification allows patients to undergo treatment or modify their surroundings for fall prevention. As explained in Chapter 1 & 2, measures of *bone quantity* have been shown to be imperfect predictors of fracture risk, and recent studies have addressed this by considering measures of *bone quality.* However, to date most measures of bone quality have focused on the macroscopic 3-D architectural parameters of the trabeculae, while the implications of the BSU that constitute the trabeculae have been largely ignored. This issue has been addressed in Chapter 4 by measuring changes in the size of BSU with age and architecture. This final chapter presents a discussion of the implications of BSU changes, the contributions that this thesis makes to literature, and its conclusions.

5.2 Intact BSU (BSU_{new})

This sub-study set out to quantify changes in the size of only the intact surface BSU with age and with 3-D architectural parameters. A significant difference was found between the distribution of BSU_{new}.A, BSU_{new}.Th, and BSU_{new}.L between the young and old groups, where the old group had smaller values for all three of the 2-D parameters. Additionally, they were found to be significantly linearly correlated with age, BV/TV, and SMI; however, no significant correlations were found with the other 3-D architectural parameters.

These results agree with earlier studies that found BSU thickness decreases with age [26,28–31]. That this agreement occurred despite methodological differences in thickness measurement (MWT vs. inscribed circle), differences in site (iliac crest vs. lumbar vertebrae), and populations (male and female vs. female only), suggests the change with age is robust.

The current work provides additional insight into the morphometric changes, showing that the length and area of the BSU also decrease with age. One known study has measured the

length of BSU at the BSU/marrow interface in the iliac crest of males and females aged 51-80 years. The geometric mean length was found to be 584.2 µm [55], which is more than 300% larger than the median length of the old group (177.3 µm) obtained in the current study. However, it should be noted that the values reported by Yamaguchi et al [55] included males, younger individuals, were measured in a different anatomical location, and used the interface length. The direct length measured in the present study will always be shorter than the interface length, as illustrated in Figure 5.1. Still, the difference between the direct length and interface length in this particular example is only 39%, and is no where near the 300% increase observed in the above-mentioned study.

The BSU/marrow interface length would be a useful descriptor for future studies since it is a true representation of the surface length occupied by new bone. Unfortunately, measuring the BSU/marrow interface length was not performed in this study because it would have required a second tracing in addition to the BSU perimeters. Thus, direct length was chosen as a compromise, to allow time for other parameters to be measured and reported for the first time. It might be possible in the future, however, to write a custom plugin for ImageJ that would calculate this value based on the overlap of the traces of the BSU and the trabecular profile perimeters.

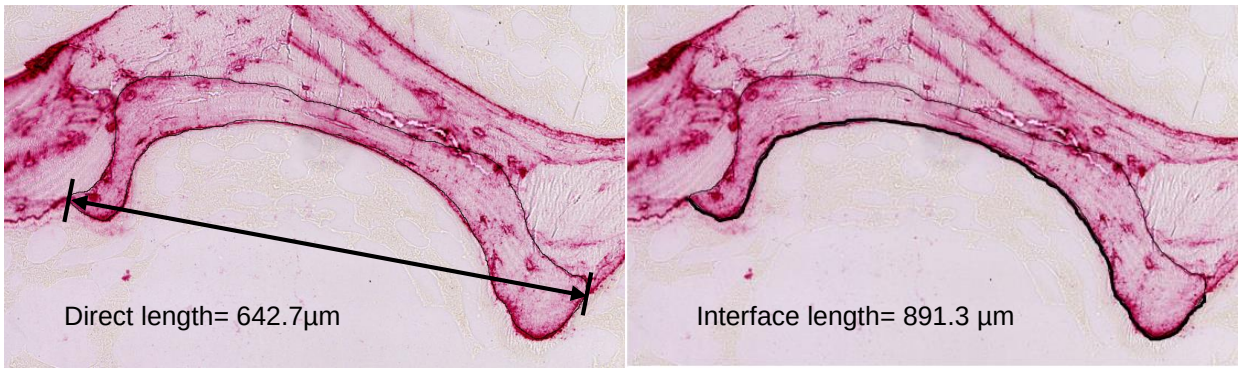

Figure 5.1: A comparison between direct length and interface length measurements.

In another study by Ohno and colleagues, morphometric changes in BSU with age in the iliac crest of women aged 12-77 years were observed [82]. Their methods of obtaining the

measurements, however, are unclear and seem to be inferential. The perimeter of each BSU was measured under polarized light microscopy, which allowed for the area to be measured. The thickness was not measured directly, but instead was estimated as the area divided by half the perimeter. The area and thickness appeared to decrease with age; however, this method of measuring BSU thickness is flawed, and biases towards smaller thicknesses due to the crescent shape of BSU. To illustrate this bias, three surface BSU from a trabecular profile were traced (Figure 5.2), and their thicknesses were estimated by the Ohno method outlined above, as well as measured by the maximum inscribed circle. It was found that when thickness was measured as the area divided by half the perimeter, the thicknesses were 46-94% smaller than those measured by maximum inscribed circle.

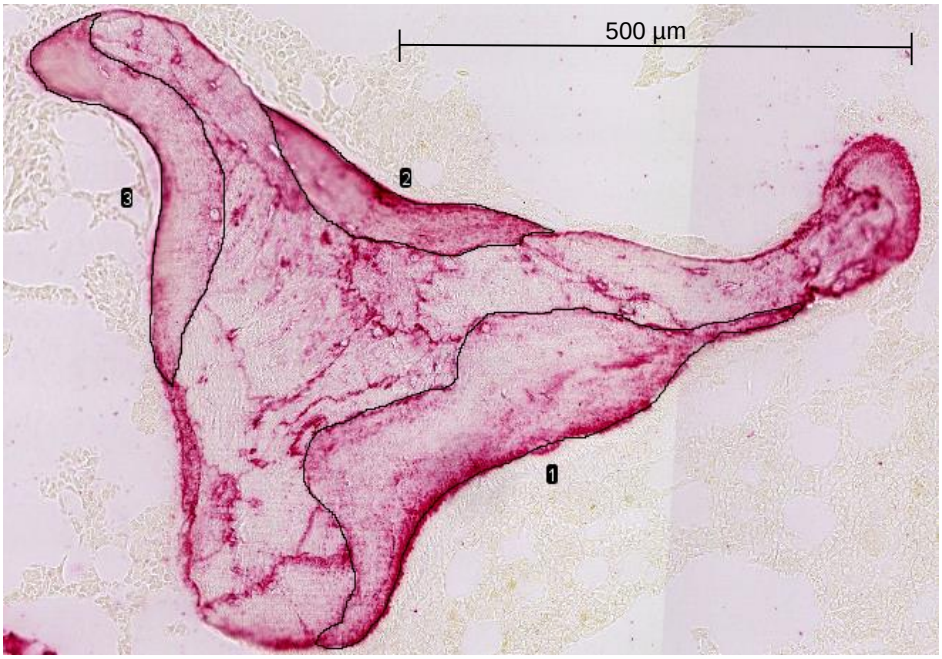

Figure 5.2: Three surface BSU used to compare methods of measuring BSU thickness

The fact that the mean BSU thickness values obtained in the Ohno study are underestimates of thickness and were still larger than the medians obtained in the current study (~52 µm vs. ~39 µm), coupled with the much larger BSU areas they reported (~45,600 μm^2 vs. ~6,300 μm^2) [82], and larger BSU lengths in the Yamaguchi study [55], would suggest that BSU

in the iliac crest are much larger than those in the lumbar vertebra. The possibility of site-dependent differences in BSU morphometry raises some interesting questions about skeletal variability in remodelling activity. These differences warrant further investigation.

It is well established that the rate of new bone deposition decreases with age in both cortical [97] and cancellous bone [27,28,31], and the results obtained in this sub-study suggest that this decrease is associated with smaller trabecular BSU in the latter. A reduction either in the number of osteoblast precursor cells, in the amount of osteoid produced by individual cells, or in the lifespan of osteoblasts are presumed to be responsible for the decreased amount of bone being formed with age [98].

A strong correlation between BSU morphometry and trabecular architecture is also shown for the first time. It is well known that BV/TV decrease with age [5,14,15] as bone is lost while SMI increases with age [5,7,13,16] as the architecture becomes more plate-like; these trends have also been observed in the current study. Though BV/TV, SMI, and age were all related to the reduction in $BSU.A_{new}$, $BSU.Th_{new}$, and $BSU.L_{new}$, stronger correlations were observed with the overall BV/TV and SMI than with age. However, it is unclear whether a low BV/TV and high SMI are the cause, or the results, of having smaller BSU.

It should be noted that, since its introduction [79], SMI has been used to quantify whether cancellous bone architecture is more plate-like (closer to zero) or rod-like (closer to three). Unfortunately, it has recently been observed that SMI is not a good predictor of the plate/rod description as it is strongly influenced by BV/TV, and does not account for the high fraction of concave surfaces that accompany a high BV/TV [80]. It is used herein for historical reasons and also because the BV/TV from the samples are low enough that the results should not be too biased.

The lack of significant relationship between BSU_{new}.Th and Tb.Th could mean that as the newly remodeled BSU become thinner with age, the trabeculae are not thinning at a proportionate

rate. This would suggest that there is not only a reduction in the amount of bone being laid down with age, but there is likely also a decrease in the erosion depth. Contrary to the hypothesis of many prior studies [28–30], this scenario wouldn't produce a large net bone loss. This concept is depicted in Figure 5.3

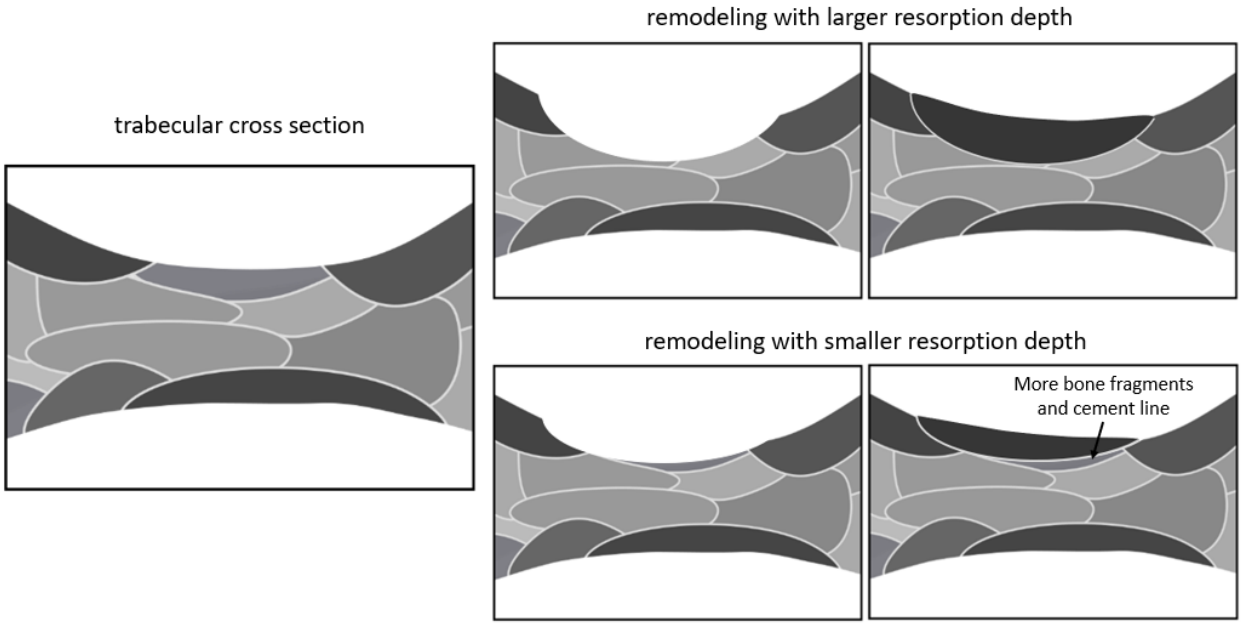

Figure 5.3: Depiction of the effects of smaller resorption depths and smaller BSU while maintaining constant trabecular thickness.

In this scenario, the trabecular thickness remains roughly the same, while the number of BSU and the amount of cement line increase, and BSU thickness decreases. Alternatively, it is possible that a relationship is present, but wasn't detected statistically due to the low number of individuals analyzed. This concept will be revisited in the following section, where the effects of thinner BSU_{new} on all BSU in the trabecular cross section will be discussed.

None of the BSU_{new} shape descriptors were related to age. Though no changes in the aspect ratio, circularity, or solidity were necessarily expected, there was a possibility that the shape of the BSU would be altered by changes in the remodeling process; however, no changes were found.

Aspect ratio was measured as the ratio of the direct length of the BSU to its thickness measured as the diameter of the maximum inscribed circle. The fact that aspect ratio didn't change with age indicates that as the BSU are becoming thinner, the length is decreasing proportionately. Circularity, which was calculated as a function of the perimeter and the area of the BSU, is a measure of compactness. Having a more scalloped cement line would increase the perimeter, without proportionately increasing the area, and thus reducing the circularity. Because of this dependence, circularity is probably an imperfect descriptor for the true compactness of BSU, as true changes in the circularity that may be occurring could be obscured by an irregular cement line. Finally, solidity is indicative of the concavity of the BSU. Since BSU become thinner with age, the resorption process is likely also affected. The fact that solidity was not different between the two aged groups could mean one of two things; either the crescent-like shape of the BSU and resorption cavity that precedes it is constant with age, or alternatively, there is so much variability in the shapes of BSU in the 2-D sections that any small differences were undetectable. Both effects could also be responsible. Some examples of the variability in the shape of BSU_{new} are illustrated in Figure 5.4

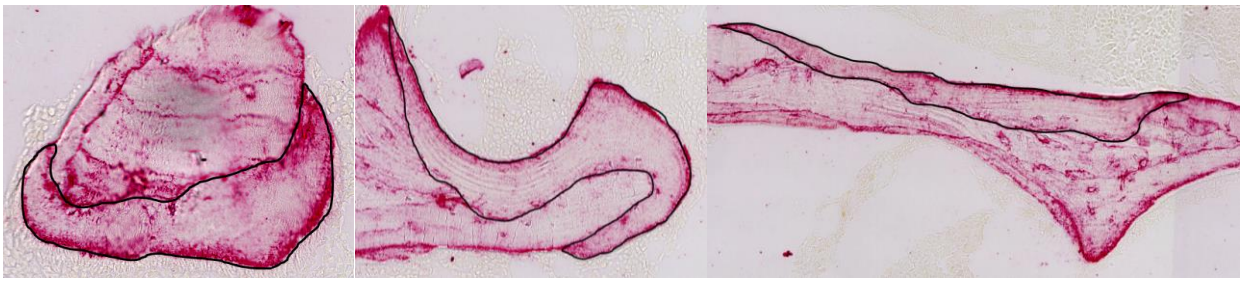

Figure 5.4: Examples of the variability in the shape of BSU_{new}.

The fact that the shapes of BSU were not found to change could also be due to shortcomings of the shape descriptors used. These three shape descriptors were selected because they were already part of ImageJ's analysis capabilities. Other potential descriptors which could give more insight into changes in the newest remodeling event with age include the moment (or center of gravity) of the BSU, the degree to which the cement line surrounding each

BSU is scalloped, the orientation of the BSU relative to trabecular orientation, and the percentage of surface area occupied by new BSU; however, these would require significant programming and implementation time.

5.3 All BSU

The second study set out to quantify changes in the morphometry of all BSU within the analysis area with age and with 3-D architectural parameters. When BSU size was analyzed as a function of age, BSU.P and BSU.L were the only parameter exhibiting a significant decrease, both when assessed via the mixed-effects analysis and using the linear regression. Again, BSU aspect ratio, circularity, and solidity were not affected by age.

Contrary to the sub-study involving only the intact surface BSU, no significant correlation or difference was found between either BSU.A or BSU.Th with age. This result makes sense because BSU_{new} reflects only the most recent BSU that are being deposited at that specific time in the individual's skeletal history. When all BSU are examined, they represent an overview of the cumulative remodeling events throughout the individual's entire life. The size and shapes of these BSU will not only be a function of how much tissue was deposited, but also how much and where tissue has been removed.

The consequences of a reduction in BSU_{new}.A, BSU_{new}.Th, and BSU_{new}.L were apparent when the #BSU/TP.A and CL.L/TP.A were examined. The reduction in the size of bone being formed at remodeling sites appears to lead to an increase in the number of BSU per unit area, and consequently, to an increase in the length of cement line per unit area in the old group. Though linear regression revealed a significant increase with age in #BSU/TP.A, no significant correlation was found with CL.L/TP.A.

The increase in #BSU/TP.A and the associated increase in CL.L/TP.A in the old group could have substantial implications for fracture risk. Though the cement line material is not yet well understood, its hypermineralization compared to the surrounding bone is thought to make it

hard and brittle [23,24]. In a cortical bone study, an increase in the number of osteons per mm^2 resulted in a lower ultimate tensile strength, which the authors attributed to an increased amount of brittle cement line that accompanies an increased number of osteons [32]. In finite element modeling of cortical bone, an increase in the strength or a decrease in the toughness of the cement line (consistent with a hard and brittle material) was found to decrease the load required for crack initiation [35]. When investigated in 2-D, a high cement line stiffness, strength, and low toughness promoted crack penetration directly though the osteons of cortical bone [34]. These results suggest that, if cement line is in fact hard and brittle, and thus stiffer and less tough than the surrounding bone, its increased presence in cancellous bone could make it more susceptible to cracks and fracture.

All three parameters of BSU size and both of the derived parameters were significantly linearly correlated to BV/TV, and even more highly correlated to SMI. The fact that these linear relationships were found with 3-D µCT parameters, but not with age (aside from BSU.L and #BSU/TP.A), means that architectural parameters, rather than age, are better predictors of bone quality at the BSU level. The relationship between BSU morphometry and 3-D architectural parameters may potentially be used for clinical investigation of fracture risk. If both architecture and the observed changes in BSU parameters are found to negatively impact cancellous bone's mechanical properties, assessment of patients' 3-D architectural parameters could potentially be used to infer these BSU parameters. Non-invasive methods, such as magnetic resonance imaging (MRI) and µCT can be used to determine cancellous bone architecture *in vivo* [74,99,100]. However, for this inference to be valid, the relationship between BSU parameters and architectural parameters would need to be proven across different skeletal sites, and in the presence of disease and drug treatment.

Interestingly, a significant positive relationship was found between Tb.Th and BSU.Th, but not with any other 2-D parameters. When considering all BSU throughout the trabeculae, Tb.Th

decreases at a rate of 6.7 µm per 1 µm decrease in BSU.Th. This finding is contrary to what was discussed in the previous section, where BSU_{new}.Th was found to be independent of Tb.Th. The reason for this apparent contradiction is that the two BSU.Th values represent different things. BSU_{new}.Th decreased independent of 3-D Tb.Th because it indicates the thickness of only the most recently remodeled tissue. The thickness of all BSU in a trabecular profile will be the result of not just the most recent remodeling event, but the cumulative history of all remodeling that has taken place. That a relationship was found when considering all BSU could simply be a reflection of the complex remodeling history (depicted in Figure 5.3). The fact that BSU_{new}.Th was not correlated to Tb.Th, and that Tb.Th decreases at a rate much higher than BSU.Th, suggests that a reduction in the thickness of BSU is not the main mechanism responsible for loss of Tb.Th with age.

When BSU.Th was normalized by Tb.Th, the relationship to age and SMI became stronger; however, the relationship to BV/TV did not. This trend results from the fact that the architecture becomes more rod-like with age (i.e., SMI increases). Rod-like trabeculae are thinner than plate-like trabeculae, so a correlation between age, SMI and Tb.Th would be expected.

The results found when considering all BSU underscores the fact that looking at only the most recently formed BSU, as was done in prior studies, does not give enough information on the overall changes in BSU with age or 3-D architectural parameters in cancellous bone.

5.4 Limitations

This study has a few limitations that bear consideration. First, the 2-D measurements reported herein do not necessarily reflect the complexity of the true 3-D BSU morphometry. Any BSU that wraps around the periphery of a rod-like trabecula, for example, has the possibility of being sectioned such that it appears as two separate BSU, leading to an underestimation of the actual area, thickness and length, and an apparent increase in the number of BSU measured.

Similarly, both the trabeculae and the BSU are anisotropic, and their orientations relative to the sectioning plane can result in over- or under-estimations of the measurements.

An additional limitation to consider is that the physical activity level of the individuals studied are unknown. As discussed in section 2.1.3, the bone's ability to adapt to its mechanical loading demands means that individuals who have lower levels of physical activity are more likely to have decreased bone mass. The effects of physical activity on BSU morphometry are unknown, but may be responsible for the apparent outliers observed in the linear regression analysis.

Manual tracing of the BSU will also incorporate some subjectivity into the results. This effect should be minimized in the current study by having a single operator perform all the measurements, and by the high resolution of the scans relative to the size of the features being measured, but cannot be completely eliminated. Nevertheless, the repeatability study suggests that that magnitude of the uncertainty associated with the measures is less than 5% in all cases. This upper limit is well below the 15% difference found in significant cases. Operator-effects should not have any effects on the trends or results reported.

Finally, a definitive connection between the observed changes and the mechanical properties has not yet been shown. The current study has demonstrated that significant changes in the size and populations of BSU in trabecular bone can develop as a function of age and changing architecture. Although arguments have been proposed about the consequences of these changes on the mechanical and failure behavior, a causal link has not been established. Finite element modeling could be used to further investigate these effects; however, experimental testing capable of separating the contributions of architecture and BSU morphometry is needed to show a definitive effect. Nevertheless, the fact that significant changes are observed is an important first step to establishing the mechanistic consequences.

5.5 Future work

Future work which would address some of these limitations would be to expand our understanding on changes in BSU morphometry for different populations. As previously mentioned, demonstrating that the relationship between BSU morphometry and architecture still holds across skeletal sites, and with disease or drug treatment, could allow for BSU parameters to be inferred non-invasively from trabecular architecture. BSU morphometry could also be compared between individuals who sustained an age-related fracture with a healthy BMD, and young controls with the same BMD. This would allow for the inadequacies of BMD measures alone to be quantified, and the BSU morphometry to be compared.

One way of achieving these goals would be using animal models which would allow for BSU morphometry to be compared across skeletal sites, and to investigate the impacts of disease and drug treatment on BSU morphometry. The mechanical implications of these differences could then be quantified with benchtop testing. This would allow for a relationship between BSU in different skeletal sites, and its dependence on other factors, to be investigated in a systematic way.

One of the technical challenges associated with future BSU studies is the extremely time-consuming task of manually tracing the BSU. The fact that BSU have largely been ignored for the past 30 years is likely due to these challenges. Although the use of modern image analysis software presents many advantages over traditional stereological techniques, any speed or efficiency improvements would increase the utility and adoption of these measurements. Future studies of this sort would strongly benefit from an automated image analysis process, which would not only drastically reduce processing time, but also eliminate subjectivity, and increase repeatability. Segmentation algorithms or AI-assisted BSU identification should be investigated.

Furthermore, in order to determine if changes in the proportions of cement line would negatively affect cancellous bone fracture behavior, the properties of cement line must first be

established. This can be done my micro-indentation, and obtaining properties for hardness and Young's modulus would allow for the cement line to be properly represented in FEM.

Finally, to truly understand the morphometric changes, the true 3-D BSU geometry needs to be quantified by reconstruction from serial sections. This would provide true data on BSU thickness, length, and volume as well as the orientation of the BSU relative to the trabecular architecture. Information on the 3-D BSU morphometry and the material properties of cement line would then permit the creation of representative FEM models, so that the mechanical implications of the changes observed can be quantified.

5.6 Contributions and conclusions

While recognizing the limitations described above, this thesis has made several contributions to the field of cancellous bone research:

1. **Additional measures of BSU morphometry:** This study has expanded on prior work which measured age-related changes in the thickness of unaltered surface BSU, by also measuring their area, length, and shape. It was found that, in addition to thickness, the area and length of BSU also decrease with age, though the shape of BSU does not change.
2. **Measures of all BSU:** The current study is the first to measure morphometric changes in all BSU throughout the trabecular cross section, rather than only those at the trabecular surface. These data provide a more comprehensive overview of the cumulative changes in BSU with age and allow for important parameters such as the number of BSU per unit area and the length of cement line per unit area to be determined.
3. **Relationship between BSU morphometry and architecture:** Relationships between BSU morphometry and 3-D architectural parameters were identified for the first time. It was found that the BV/TV and SMI were better predictors of BSU morphometry than age.

In summary, new methods have been developed to allow for BSU morphometric parameters to be measured, and it was established that changes in BSU morphometry occur both with age and with architectural deterioration. Though the implications of these changes have not been demonstrated, the work presented sets the stage for a new branch of cancellous bone quality research, which may include comparative studies between sexes, disease, and drug treatments.

References

[1] World Health Organization. WHO scientific group on the assessment of osteoporosis at primary health care level. Brussels, Belgium: 2004.

[2] Hopkins RB, Burke N, Von Keyserlingk C, Leslie WD, Morin SN, Adachi JD, et al. The current economic burden of illness of osteoporosis in Canada. Osteoporos Int 2016;27:3023–32. https://doi.org/10.1007/s00198-016-3631-6.

[3] Burge R, Dawson-Hughes B, Solomon DH, Wong JB, King A, Tosteson A. Incidence and economic burden of osteoporosis-related fractures in the United States, 2005-2025. J Bone Miner Res 2007;22:465–75. https://doi.org/10.1359/jbmr.061113.

[4] Currey JD. Bones: Structure and Mechanics. Princeton University Press; 2002.

[5] Chen H, Zhou X, Fujita H, Onozuka M, Kubo K-Y. Age-Related Changes in Trabecular and Cortical Bone Microstructure. Int J Endocrinol 2013;2013:e213234. https://doi.org/10.1155/2013/213234.

[6] Modic changes. Marcaurel n.d. http://www.marcaurel.com.au/modic-changes/ (accessed June 24, 2020).

[7] Mittra E, Rubin C, Gruber B, Qin Y-X. Evaluation of trabecular mechanical and microstructural properties in human calcaneal bone of advanced age using mechanical testing, CT, and DXA. J Biomech 2008;41:368–75. https://doi.org/10.1016/j.jbiomech.2007.09.003.

[8] Mosekilde L. Vertebral structure and strength in vivo and in vitro. Calcif Tissue Int 1993;53 Suppl 1:S121-125; discussion S125-126. https://doi.org/10.1007/bf01673420.

[9] NIH Consensus Development Panel on Osteoporosis Prevention, Diagnosis, and Therapy. Osteoporosis prevention, diagnosis, and therapy. JAMA 2001;285:785–95. https://doi.org/10.1001/jama.285.6.785.

[10] Alswat KA. Gender Disparities in Osteoporosis. J Clin Med Res 2017;9:382–7. https://doi.org/10.14740/jocmr2970w.

[11] Pasco JA, Seeman E, Henry MJ, Merriman EN, Nicholson GC, Kotowicz MA. The population burden of fractures originates in women with osteopenia, not osteoporosis. Osteoporos Int 2006;17:1404–9. https://doi.org/10.1007/s00198-006-0135-9.

[12] Cui W-Q, Won Y-Y, Baek M-H, Lee D-H, Chung Y-S, Hur J-H, et al. Age-and region-dependent changes in three-dimensional microstructural properties of proximal femoral trabeculae. Osteoporos Int 2008;19:1579–87. https://doi.org/10.1007/s00198-008-0601-7.

[13] Ding M, Hvid I. Quantification of age-related changes in the structure model type and trabecular thickness of human tibial cancellous bone. Bone 2000;26:291–5. https://doi.org/10.1016/s8756-3282(99)00281-1.

[14] Macdonald HM, Nishiyama KK, Kang J, Hanley DA, Boyd SK. Age-related patterns of trabecular and cortical bone loss differ between sexes and skeletal sites: a population-based HR-pQCT study. J Bone Miner Res 2011;26:50–62. https://doi.org/10.1002/jbmr.171.

[15] Gong H, Zhang M, Yeung HY, Qin L. Regional variations in microstructural properties of vertebral trabeculae with aging. J Bone Miner Metab 2005;23:174–80. https://doi.org/10.1007/s00774-004-0557-4.

[16] Chen H, Shoumura S, Emura S, Bunai Y. Regional variations of vertebral trabecular bone microstructure with age and gender. Osteoporos Int 2008;19:1473–83. https://doi.org/10.1007/s00198-008-0593-3.

[17] Sabet FA, Raeisi Najafi A, Hamed E, Jasiuk I. Modelling of bone fracture and strength at different length scales: a review. Interface Focus 2016;6. https://doi.org/10.1098/rsfs.2015.0055.

[18] Grynpas M. Age and disease-related changes in the mineral of bone. Calcif Tissue Int 1993;53 Suppl 1:S57-64. https://doi.org/10.1007/bf01673403.

[19] Wang X, Shen X, Li X, Mauli Agrawal C. Age-related changes in the collagen network and toughness of bone. Bone 2002;31:1–7. https://doi.org/10.1016/S8756-3282(01)00697-4.

[20] Zioupos P, Currey JD, Hamer AJ. The role of collagen in the declining mechanical properties of aging human cortical bone. J Biomed Mater Res 1999;45:108–16. https://doi.org/10.1002/(SICI)1097-4636(199905)45:2<108::AID-JBM5>3.0.CO;2-A.

[21] Currey JD. Changes in the impact energy absorption of bone with age. J Biomech 1979;12:459–69. https://doi.org/10.1016/0021-9290(79)90031-9.

[22] Hamed E, Jasiuk I, Yoo A, Lee Y, Liszka T. Multi-scale modelling of elastic moduli of trabecular bone. J R Soc Interface 2012;9:1654–73. https://doi.org/10.1098/rsif.2011.0814.

[23] Smith JW. Age changes in the organic fraction of bone. J Bone Joint Surg 1963;45-B:761–9. https://doi.org/10.1302/0301-620X.45B4.761.

[24] Skedros JG, Holmes JL, Vajda EG, Bloebaum RD. Cement lines of secondary osteons in human bone are not mineral-deficient: New data in a historical perspective. Anat Rec A Discov Mol Cell Evol Biol 2005;286A:781–803. https://doi.org/10.1002/ar.a.20214.

[25] Choi K, Goldstein SA. A comparison of the fatigue behavior of human trabecular and cortical bone tissue. J Biomech 1992;25:1371–81. https://doi.org/10.1016/0021-9290(92)90051-2.

[26] Croucher PI, Mellish RW, Vedi S, Garrahan NJ, Compston JE. The relationship between resorption depth and mean interstitial bone thickness: age-related changes in man. Calcif Tissue Int 1989;45:15–9. https://doi.org/10.1007/BF02556655.

[27] Darby AJ, Meunier PJ. Mean wall thickness and formation periods of trabecular bone packets in idiopathic osteoporosis. Calcif Tissue Int 1981;33:199–204. https://doi.org/10.1007/BF02409438.

[28] Dempster DW, Arlot MA, Meunier PJ. Mean wall thickness and formation periods of trabecular bone packets in corticosteroid-induced osteoporosis. Calcif Tissue Int 1983;35:410–7. https://doi.org/10.1007/BF02405069.

[29] Kragstrup J, Melsen F, Mosekilde L. Thickness of bone formed at remodeling sites in normal human iliac trabecular bone: variations with age and sex. Metab Bone Dis Relat Res 1983;5:17–21. https://doi.org/10.1016/0221-8747(83)90046-2.

[30] Lips P, Courpron P, Meunier P. Mean Wall Thickness of Trabecular Bone Packets in Human Iliac Crest - Changes with Age. Calcif Tissue Int 1978;26:13–7. https://doi.org/10.1007/BF02013227.

[31] Vedi S, Compston JE, Webb A, Tighe JR. Histomorphometric analysis of dynamic parameters of trabecular bone formation in the iliac crest of Normal British subjects. Metab Bone Dis Relat Res 1983;5:69–74. https://doi.org/10.1016/0221-8747(83)90004-8.

[32] Evans FG, Bang S. Differences and relationships between the physical properties and the microscopic structure of human femoral, tibial and fibular cortical bone. Am j Anat 1967;120:79–88. https://doi.org/10.1002/aja.1001200107.

[33] Yeni YN, Brown CU, Wang Z, Norman TL. The influence of bone morphology on fracture toughness of the human femur and tibia. Bone 1997;21:453–9. https://doi.org/10.1016/S8756-3282(97)00173-7.

[34] Gustafsson A, Wallin M, Khayyeri H, Isaksson H. Crack propagation in cortical bone is affected by the characteristics of the cement line: a parameter study using an XFEM interface damage model. Biomech Model Mechanobiol 2019;18:1247–61. https://doi.org/10.1007/s10237-019-01142-4.

[35] Ural A, Mischinski S. Multiscale modeling of bone fracture using cohesive finite elements. Eng Fract Mech 2013;103:141–52. https://doi.org/10.1016/j.engfracmech.2012.05.008.

[36] Wang M, Li S, Scheidt A vom, Qwamizadeh M, Busse B, Silberschmidt VV. Numerical study of crack initiation and growth in human cortical bone: Effect of micro-morphology. Eng Fract Mech 2020;232:107051. https://doi.org/10.1016/j.engfracmech.2020.107051.

[37] Chan KS, Chan CK, Nicolella DP. Relating Crack-tip Deformation to Mineralization and Fracture Resistance in Human Femur Cortical Bone. Bone 2009;45:427–34. https://doi.org/10.1016/j.bone.2009.01.468.

[38] Thomsen JS, Jensen MV, Niklassen AS, Ebbesen EN, Brüel A. Age-related changes in vertebral and iliac crest 3D bone microstructure--differences and similarities. Osteoporos Int 2015;26:219–28. https://doi.org/10.1007/s00198-014-2851-x.

[39] Weiner S, Wagner HD. THE MATERIAL BONE: Structure-Mechanical Function Relations. Annu Rev Mater Sci 1998;28:271–98. https://doi.org/10.1146/annurev.matsci.28.1.271.

[40] Webster SSJ. Integrated Bone Tissue Physiology: Anatomy and Physiology. Bone Mechanics Handbook. Second, New York: Informa Healthcare USA Inc.; 2009.

[41] Singh I. The architecture of cancellous bone. J Anat 1978;127:305–10.

[42] Goda I, Ganghoffer J-F. Identification of couple-stress moduli of vertebral trabecular bone based on the 3D internal architectures. J Mech Behav Biomed Mater 2015;51:99–118. https://doi.org/10.1016/j.jmbbm.2015.06.036.

[43] Rho JY, Kuhn-Spearing L, Zioupos P. Mechanical properties and the hierarchical structure of bone. Med Eng Phys 1998;20:92–102. https://doi.org/10.1016/s1350-4533(98)00007-1.

[44] Fratzl P, Gupta H, Paschalis L, Roschger P. Structure and mechanical quality of the collagen-mineral nano-composite in bone. J Mater Chem 2004;14. https://doi.org/10.1039/B402005G.

[45] Ciarelli TE, Fyhrie DP, Parfitt AM. Effects of vertebral bone fragility and bone formation rate on the mineralization levels of cancellous bone from white females. Bone 2003;32:311–5. https://doi.org/10.1016/S8756-3282(02)00975-4.

[46] Dempster DW, Lindsay R. Pathogenesis of osteoporosis. Lancet 1993;341:797–801. https://doi.org/10.1016/0140-6736(93)90570-7.

[47] Dempster DW. Bone remodeling. Disorders of bone and mineral metabolism., New York: Raven; 1992, p. 335.

[48] Orwoll ES, Adler RA, Amin S, Binkley N, Lewiecki EM, Petak SM, et al. Skeletal health in long-duration astronauts: Nature, assessment, and management recommendations from the NASA bone summit. J Bone Miner Res 2013;28:1243–55. https://doi.org/10.1002/jbmr.1948.

[49] Krahl H, Michaelis U, Pieper H-G, Quack G, Montag M. Stimulation of Bone Growth Through Sports: A Radiologic Investigation of the Upper Extremities in Professional Tennis Players. Am J Sports Med 1994;22:751–7. https://doi.org/10.1177/036354659402200605.

[50] Majeska R. Cell Biology of Bone. Bone Mechanics Handbook. Second, New York: Informa Healthcare USA Inc.; 2009.

[51] Delaisse J-M. The reversal phase of the bone-remodeling cycle: cellular prerequisites for coupling resorption and formation. BoneKEy Reports 2014;3. https://doi.org/10.1038/bonekey.2014.56.

[52] Cowin S, Moss M. Mechanosensory Mechanisms in Bone. Bone Mechanics Handbook. Second, New York: Informa Healthcare USA Inc.; 2009.

[53] Parfitt AM. Osteonal and hemi-osteonal remodeling: The spatial and temporal framework for signal traffic in adult human bone. J Cell Biochem 1994;55:273–86. https://doi.org/10.1002/jcb.240550303.

[54] Lisowska B, Kosson D, Domaracka K. Lights and shadows of NSAIDs in bone healing: the role of prostaglandins in bone metabolism. Drug Des Devel Ther 2018;12:1753–8. https://doi.org/10.2147/DDDT.S164562.

[55] Yamaguchi K, Croucher PI, Compston JE. Comparison between the lengths of individual osteoid seams and resorption cavities in human iliac crest cancellous bone. J Bone Miner Res 1993;23:27–33. https://doi.org/10.1016/S0169-6009(08)80088-8.

[56] Bloebaum RD, Skedros JG, Vajda EG, Bachus KN, Constantz BR. Determining mineral content variations in bone using backscattered electron imaging. Bone 1997;20:485–90. https://doi.org/10.1016/s8756-3282(97)00015-x.

[57] Smith LJ, Schirer JP, Fazzalari NL. The role of mineral content in determining the micromechanical properties of discrete trabecular bone remodeling packets. J Biomech 2010;43:3144–9. https://doi.org/10.1016/j.jbiomech.2010.07.038.

[58] Mckee MD, Nanci A. Osteopontin: An Interfacial Extracellular Matrix Protein in Mineralized Tissues. Connect Tissue Res 1996;35:197–205. https://doi.org/10.3109/03008209609029192.

[59] Augat P, Weyand D, Panzer S, Klier T. Osteoporosis prevalence and fracture characteristics in elderly female patients with fractures. Arch Orthop Trauma Surg 2010;130:1405–10. https://doi.org/10.1007/s00402-010-1142-z.

[60] Schaffler MB, Choi K, Milgrom C. Aging and matrix microdamage accumulation in human compact bone. Bone 1995;17:521–5. https://doi.org/10.1016/8756-3282(95)00370-3.

[61] Fan R, Gong H, Zhang X, Liu J, Jia Z, Zhu D. Modeling the Mechanical Consequences of Age-Related Trabecular Bone Loss by XFEM Simulation. Comput Math Methods Med 2016;2016:1–12. https://doi.org/10.1155/2016/3495152.

[62] Hallberg I, Rosenqvist AM, Kartous L, Löfman O, Wahlström O, Toss G. Health-related quality of life after osteoporotic fractures. Osteoporos Int 2004;15:834–41. https://doi.org/10.1007/s00198-004-1622-5.

[63] O'Flaherty E. Modeling Normal Aging Bone Loss, with Consideration of Bone Loss in Osteoporosis. Toxicol Sci 2020;55:171–88. https://doi.org/10.1093/toxsci/55.1.171.

[64] Chappard D, Baslé M-F, Legrand E, Audran M. Trabecular bone microarchitecture: a review. Morphologie 2008;92:162–70. https://doi.org/10.1016/j.morpho.2008.10.003.

[65] EUROSPINE Patient Line - Osteoporosis - Introduction n.d. https://www.eurospinepatientline.org/en/osteoporosis---introduction.htm (accessed March 2, 2020).

[66] Parfitt AM, Mathews CH, Villanueva AR, Kleerekoper M, Frame B, Rao DS. Relationships between surface, volume, and thickness of iliac trabecular bone in aging and in osteoporosis. Implications for the microanatomic and cellular mechanisms of bone loss. J Clin Invest 1983;72:1396–409.

[67] Thomsen JS, Laib A, Koller B, Prohaska S, Mosekilde L, Gowin W. Stereological measures of trabecular bone structure: comparison of 3D micro computed tomography with 2D histological sections in human proximal tibial bone biopsies. J Microsc 2005;218:171–9. https://doi.org/10.1111/j.1365-2818.2005.01469.x.

[68] McCalden RW, McGeough JA, Court-Brown CM. Age-related changes in the compressive strength of cancellous bone. The relative importance of changes in density and trabecular architecture. J Bone Joint Surg Am 1997;79:421–7. https://doi.org/10.2106/00004623-199703000-00016.

[69] Khosla S, Riggs BL, Atkinson EJ, Oberg AL, McDaniel LJ, Holets M, et al. Effects of Sex and Age on Bone Microstructure at the Ultradistal Radius: A Population-Based Noninvasive In Vivo Assessment. J Bone Miner Res 2006;21:124–31. https://doi.org/10.1359/JBMR.050916.

[70] Barak MM, Black MA. A novel use of 3D printing model demonstrates the effects of deteriorated trabecular bone structure on bone stiffness and strength. J Mech Behav Biomed Mater 2018;78:455–64. https://doi.org/10.1016/j.jmbbm.2017.12.010.

[71] Hildebrand T, Rüegsegger P. A new method for the model-independent assessment of thickness in three-dimensional images. J Microsc 1997;185:67–75. https://doi.org/10.1046/j.1365-2818.1997.1340694.x.

[72] Chen H, Zhou X, Shoumura S, Emura S, Bunai Y. Age- and gender-dependent changes in three-dimensional microstructure of cortical and trabecular bone at the human femoral neck. Osteoporos Int 2010;21:627–36. https://doi.org/10.1007/s00198-009-0993-z.

[73] Thomsen JS, Niklassen AS, Ebbesen EN, Brüel A. Age-related changes of vertical and horizontal lumbar vertebral trabecular 3D bone microstructure is different in women and men. Bone 2013;57:47–55. https://doi.org/10.1016/j.bone.2013.07.025.

[74] Ulrich D, van Rietbergen B, Laib A, Rüegsegger P. The ability of three-dimensional structural indices to reflect mechanical aspects of trabecular bone. Bone 1999;25:55–60. https://doi.org/10.1016/s8756-3282(99)00098-8.

[75] Bouxsein ML, Boyd SK, Christiansen BA, Guldberg RE, Jepsen KJ, Müller R. Guidelines for assessment of bone microstructure in rodents using micro–computed tomography. J Bone Miner Res 2010;25:1468–86. https://doi.org/10.1002/jbmr.141.

[76] Danielsson P-E. Euclidean distance mapping. Comput Gr Image Process 1980;14:227–48. https://doi.org/10.1016/0146-664X(80)90054-4.

[77] Silva MJ, Gibson LJ. Modeling the mechanical behavior of vertebral trabecular bone: Effects of age-related changes in microstructure. Bone 1997;21:191–9. https://doi.org/10.1016/S8756-3282(97)00100-2.

[78] Kennedy OD, Brennan O, Rackard SM, O'Brien FJ, Taylor D, Lee TC. Variation of trabecular microarchitectural parameters in cranial, caudal and mid-vertebral regions of the ovine L3 vertebra. J Anat 2009;214:729–35. https://doi.org/10.1111/j.1469-7580.2009.01054.x.

[79] Hildebrand TOR, Rüegsegger P. Quantification of Bone Microarchitecture with the Structure Model Index. Comput Methods Biomech Biomed Engin 1997;1:15–23. https://doi.org/10.1080/01495739708936692.

[80] Salmon PL, Ohlsson C, Shefelbine SJ, Doube M. Structure Model Index Does Not Measure Rods and Plates in Trabecular Bone. Front Endocrinol 2015;6. https://doi.org/10.3389/fendo.2015.00162.

[81] Kragstrup J, Melsen F, Mosekilde L. Effects of thyroid hormone(s) on mean wall thickness of trabecular bone packets. Metab Bone Dis Relat Res 1981;3:181–5. https://doi.org/10.1016/0221-8747(81)90006-0.

[82] Ohno A, Amagai H, Miyagawa S, Yoshikawa S. Mean wall thickness of iliac trabecular bone packets in 98 normal Japanese females. International Congress on Bone Morphometry, vol. 5, 1990, p. 392–5.

[83] Hammond MA, Wallace JM, Allen MR, Siegmund T. Mechanics of linear microcracking in trabecular bone. J Biomech 2019;83:34–42. https://doi.org/10.1016/j.jbiomech.2018.11.018.

[84] Thomsen JS, Ebbesen EN, Mosekilde L. A new method of comprehensive static histomorphometry applied on human lumbar vertebral cancellous bone. Bone 2000;27:129–38. https://doi.org/10.1016/S8756-3282(00)00285-4.

[85] Thomsen JS, Ebbesen EN, Mosekilde L. Zone-dependent changes in human vertebral trabecular bone: clinical implications. Bone 2002;30:664–9. https://doi.org/10.1016/S8756-3282(02)00686-5.

[86] Thomsen JS, Ebbesen EN, Mosekilde Li. Static histomorphometry of human iliac crest and vertebral trabecular bone: a comparative study. Bone 2002;30:267–74. https://doi.org/10.1016/S8756-3282(01)00666-4.

[87] Thomsen JS, Ebbesen EN, Mosekilde L i. Age-related differences between thinning of horizontal and vertical trabeculae in human lumbar bone as assessed by a new computerized method. Bone 2002;31:136–42. https://doi.org/10.1016/S8756-3282(02)00801-3.

[88] Thomsen JS, Ebbesen EN, Mosekilde Li. Predicting human vertebral bone strength by vertebral static histomorphometry. Bone 2002;30:502–8. https://doi.org/10.1016/S8756-3282(01)00702-5.

[89] Erben RG. Embedding of Bone Samples in Methylmethacrylate: An Improved Method Suitable for Bone Histomorphometry, Histochemistry, and Immunohistochemistry: J Histochem Cytochem 2016. https://doi.org/10.1177/002215549704500215.

[90] Living Well With Spondylolisthesis n.d. https://www.askdrlavine.com/livingwellwithspondylolisthesis.html (accessed June 4, 2020).

[91] The Vertebral Column - Joints - Vertebrae - Vertebral Structure n.d. https://teachmeanatomy.info/back/bones/vertebral-column/ (accessed June 4, 2020).

[92] SelectScience. NanoZoomer 2.0-HT slide scanner from Hamamatsu Photonics | SelectScience n.d. https://www.selectscience.net/products/nanozoomer-20-ht-slide-scanner/?prodID=85107 (accessed January 24, 2020).

[93] Rueden CT, Schindelin J, Hiner MC, DeZonia BE, Walter AE, Arena ET, et al. ImageJ2: ImageJ for the next generation of scientific image data. BMC Bioinformatics 2017;18:529. https://doi.org/10.1186/s12859-017-1934-z.

[94] NDP.view2 Viewing software U12388-01 n.d. https://www.hamamatsu.com/us/en/product/type/U12388-01/index.html (accessed January 24, 2020).

[95] ROI Manager. Analyze Menu n.d. https://imagej.nih.gov/ij/docs/menus/analyze.html#ap (accessed June 4, 2020).

[96] Burri O. Max Inscribed Circles. BioImaging and Optics Platform (BIOP) 2018. https://github.com/BIOP/ijp-max-inscribed-circles (accessed June 4, 2020).

[97] Frost HM. Tetracycline-based histological analysis of bone remodeling. Calc Tis Res 1969;3:211–37. https://doi.org/10.1007/BF02058664.

[98] Szulc P, Seeman E. Thinking inside and outside the envelopes of bone: dedicated to PDD. Osteoporos Int 2009;20:1281–8. https://doi.org/10.1007/s00198-009-0994-y.

[99] Majumdar S, Bay BK. Noninvasive Assessment of Trabecular Bone Architecture and The Competence of Bone. Springer Science & Business Media; 2012.

[100] Campbell GM, Sophocleous A. Quantitative analysis of bone and soft tissue by micro-computed tomography: applications to ex vivo and in vivo studies. Bonekey Rep 2014;3. https://doi.org/10.1038/bonekey.2014.59.

Appendix A: Cutting procedure

The vertebrae were sectioned using a Leica 2500 microtome at the Department of Forensic Medicine, Aarhus University, Denmark. The steps taken to prepare the vertebrae for staining are outlined below, along with pictures for visualisation and recreation.

1. The microtome was set for a cutting thickness of 7 µm and speed of around 4 mm/s.

Figure A–1: Step 1: Microtome set to 4.3mm/s cutting speed and 7µm thickness

2. A generous amount of 40% ethanol was added to the embedded vertebra's surface with a paintbrush to lubricate the surface every time a section was removed.

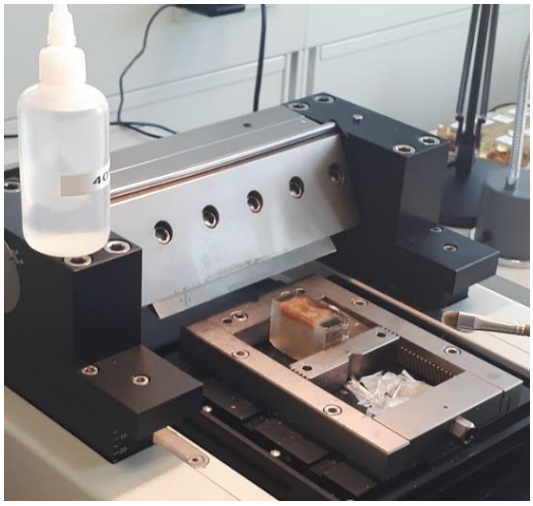

Figure A–2: Step 2: Ethanol added to surface of vertebral specimen between sections

3. As the machine was cutting, the sections were gently pulled up with the use of a paintbrush and tweezers

Figure A–3: Step 3: Sectioning of the vertebrae

4. The sections were then placed in individual water baths.

Figure A–4: Step 4: Sections placed in water baths

5. The sections were retrieved from the water baths using a microscope glass and tweezers to help orient the tissue

Figure A–5: Step 5: Sections placed onto microscope slides

6. The sections (now on microscope slides) were laid flat and dripped over with 70% alcohol.

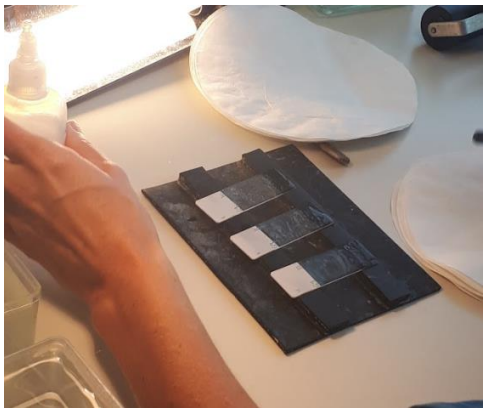

Figure A–6: Step 6: Slides dripped with alcohol

7. Thin plastic films were added to protect the exposed surface of the vertebral sections.

Figure A–7: Step 7: Plastic films added to slides

8. The white area at the top of each slide was labeled with the patient ID and the section number. Knowing the section number and the thickness of each section would allow a specific section to be located in 3-D space, for example, in the µCT scans.

9. 70% alcohol was spread over the plastic films covering the sections to remove air bubbles.

Figure A–8: Step 9: Alcohol spread over plastic films

10. The slides were placed between paper, and a roller was used to further flatten out the samples and remove air bubbles

Figure A–9: Step 10: Slides flattened with roller

11. Finally, the slides were put under pressure with parallel clamps for 14 days at 4°C before being stained to ensure proper adherence of the vertebral sections to the microscope slides.

Figure A–10: Step 11: Slides placed in parallel clamps

Appendix B: Staining procedure

The staining procedure was carried out in the laboratory of the department of Clinical Cell Biology, Pathology Research Unit, Odense University Hospital, Denmark. Multiple types of staining were tested, including Mayer's hematoxylin and Goldner's trichrome, but an osteopontin immunostaining was found to produce the best results. The steps of the osteopontin staining procedure, are included below, along with a list of the products used.

List of products:

- TBS (Tris-buffered saline) — [0.05 M Tris-HCl (pH 7.6) + 0.15 M NaCl]
- Casein (phosphoprotein)— Sigma-Aldrich; Copenhagen, Denmark
- TWEEN (viscous liquid) —Sigma-Aldrich; Copenhagen, Denmark
- Avidin/biotin blocking kit — Dako; Glostrup, Denmark
- Biotinylated goat anti-osteopontin antibody — BAF1433; R&D systems; Minneapolis, MN
- Rabbit anti-goat antibody — 305-065-046; Jackson ImmunoResearch; West Grove, PA
- BrightVision poly- alkaline phosphatase-anti-rabbit IgG — VWRKDPVO110AP; ImmunoLogic; Duiven, Netherlands
- Liquid Permanent Red kit — DAKO; Glostrup, Denmark
- Aquatex (aqueous mounting agent) — Sigma-Aldrich; Copenhagen, Denmark

Staining protocol:

1. Washing
    a. The slides were inserted in vertical pressurized capillary receptacles. Solutions dripped into the top chamber remain on the slides until it is flushed out when a new solution is added
    b. The slides were first dripped with distilled water for >5 minutes to rehydrate
    c. The slides were then dripped with TBS/TWEEN wash solution for 2x5 minutes (dripped twice, and left for five minutes each time)

Figure B–1: Step 1: Slides placed in staining receptacles

2. Blocking
    a. The slides were dripped with a solution of 0.5% casein diluted in TBS for 20 minutes
    b. Approximately 5 drops of Avidin were added to all slides for 10 minutes
    c. Slides were dripped in TBS/TWEEN wash for 2x5 minutes
    d. Approximately 5 drops of Biotin were added to all slides for 10 minutes
    e. Slides were dripped in TBS/TWEEN wash for 2x5 minutes

Figure B–2: Step 2: Avidin/Biotin blocking kit

3. Osteopontin Staining
    a. Osteopontin primary antibody was mixed with the TBS/casein solution at a 1:50 ratio.

Figure B–3: Step 3: Osteopontin primary antibody

b. Approximately 200 µL of the mixture was added to each slide

c. The slides were incubated overnight at 4°C

d. The next day, the slides were soaked in TBS/TWEEN wash for 2x5 minutes

4. Secondary antibody staining

a. Rabbit-anti-goat secondary antibody was mixed with TBS/casein at a 1:250 ratio

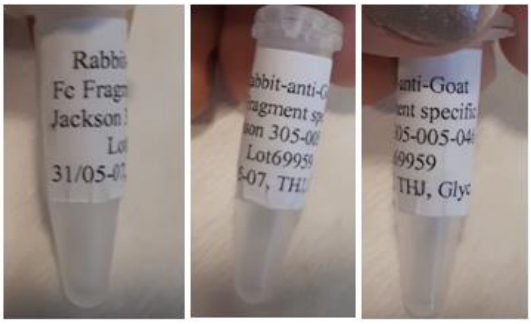

Figure B–4: Step 4: Rabbit-anti-Goat secondary antibody

b. Approximately 200 µL of the mixture was added to each slide and let sit for 2 hours

c. The slides were then dripped in TBS/TWEEN wash for 2x5 minutes

5. Detection

a. BrightVision anti-rabbit conj. AP polymer was dripped on each slide and let sit for 30 minutes

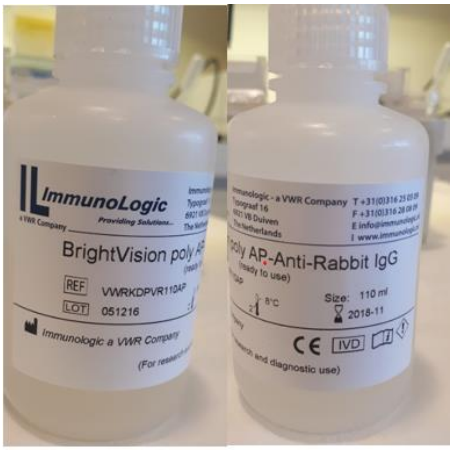

Figure B–5: Step 5: BrightVision anti-rabbit conj. AP polymer

b. The slides were dripped with TBS/TWEEN wash for 2x5 minutes

c. The slides were then soaked with distilled water for 5 minutes

6. Visualization

a. The components of the liquid permanent red solution were mixed and immediately added to the slides, and let sit for 10 minutes

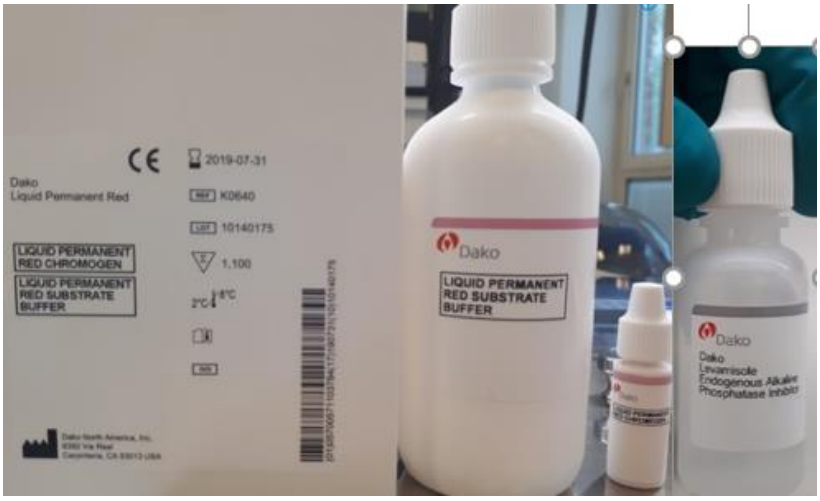

Figure B–6: Step 6: Liquid permanent red kit

b. The slides were then soaked in distilled water for 5 minutes

7. Mounting

a. The slides were removed from the pressurized capillary receptacles

b. Aquatex was applied to cover glasses, which were pressed onto the stained vertebral sections.

c. The edges of the slides were sealed with nail polish for preservation

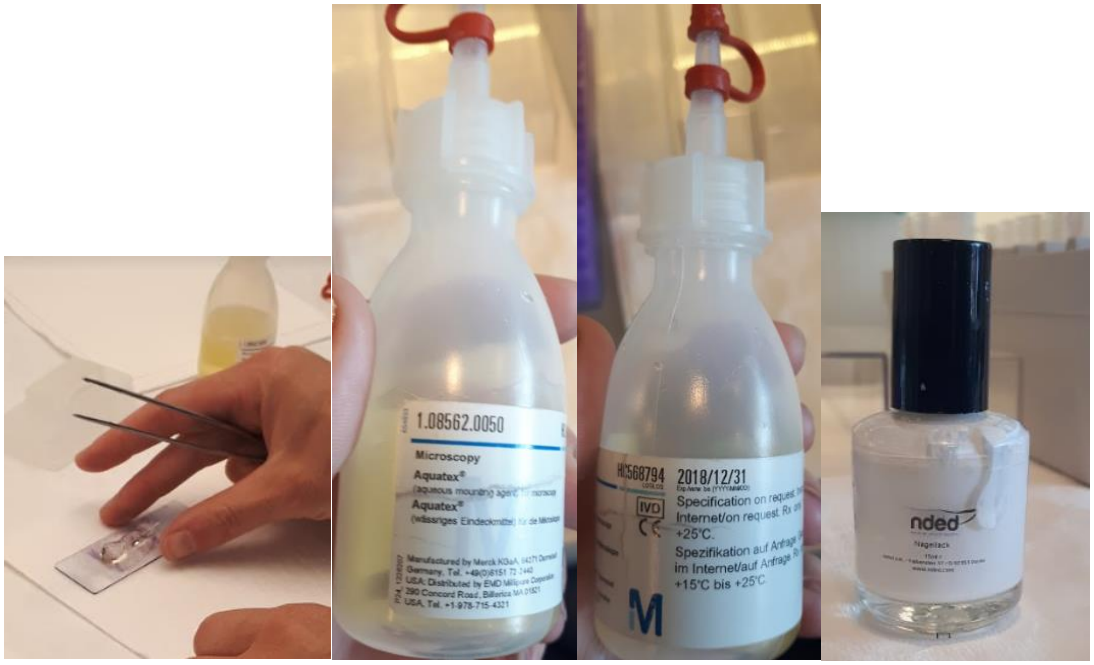

Figure B–7: Step 7: Slides mounted with Aquatex and sealed with nail polish